

The Origin and Evolution of Silica-saturated Alkalic Suites: an Experimental Study

H. NEKVASIL*, A. DONDOLINI, J. HORN, J. FILIBERTO,
H. LONG AND D. H. LINDSLEY

DEPARTMENT OF GEOSCIENCES, STATE UNIVERSITY OF NEW YORK, STONY BROOK, NY 11794-2100, USA

RECEIVED OCTOBER 6, 2002; ACCEPTED AUGUST 20, 2003

Experimental simulation of incremental crystal fractionation of a hy-normative hawaiite indicates that the spectrum of compositions from mildly alkalic hawaiite to sodic rhyolite found in silica-saturated alkalic suites of the ocean islands and continental hotspots and rifts can be produced by fractionation at 9.3 kbar with bulk water contents > ~0.5 wt % (in the hawaiite) at f_{O_2} ~1.5 log units below the fayalite–magnetite–quartz buffer (FMQ). Along this path, mildly alkalic basalt becomes increasingly alkalic because of the domination of clinopyroxene in the early fractionating assemblage and suppression of plagioclase. Kaersutite dominates at intermediate temperatures and results in stronger silica enrichment as the melt evolves to rhyolite. The fractionation assemblages are strongly pressure-sensitive. At mid-crustal pressures, melts become potassic rather than sodic. At shallow conditions, the abundance of early olivine produces strong silica enrichment and subalkalic total alkalis to silica ratios. Natural mineral assemblages from silica-saturated alkalic suites show a polybaric history with fractionation at ~30 km depth followed by decompression of liquids residual to this fractionation and crystallization, but not extensive fractionation, of lower-pressure assemblages. Equilibrium crystallization paths suggest that partial melting of hawaiite could produce the intermediate members of these suites provided that sufficient water was available in the source region.

KEY WORDS: *alkalic; experimental; fractionation; hotspot; igneous*

INTRODUCTION

Silica-saturated alkalic suites are found worldwide on the ocean islands (e.g. Ascension Island, Harris, 1983; the Samoan Islands, Macdonald, 1964; Terceira, Azores, Schmincke, 1973; Self & Gunn, 1976; White *et al.*, 1979; Mungall & Martin, 1995; Clarion Island, Mexico,

Bryan, 1967) and in continental hotspot (e.g. the Tertiary volcanic province of SE Australia, Stolz, 1985; the Massif Central, France, Downes, 1987) and rift environments (e.g. the Gardar Province, Southern Greenland, Upton & Emeleus, 1987; the Kenya rift, Macdonald, 1987). These suites contain temporally and spatially associated rocks spanning the compositional range from mildly alkalic hypersthene (hy)-normative basalt and silica-saturated alkalic intermediate rocks to alkali-rich rhyolite (Fig. 1). Characteristic of these suites is a strong increase in alkalis relative to silica in the basaltic members and its moderation at intermediate compositions (Fig. 2).

The basic trends of compositional change with silica content for all major oxides (Fig. 2) appear substantially the same for silica-saturated alkalic suites in ocean island and continental environments. The greatest diversity among the suites is found in the variation of K_2O content with silica (Fig. 2b) and hence, in Na_2O/K_2O ratios. These differences have induced some workers to subdivide the silica-saturated alkalic suites into a 'sodic' series ($Na_2O/K_2O > 2$, e.g. Ascension Island, Harris, 1983) and a 'potassic' series (with $Na_2O/K_2O < 2$; e.g. Nandewar Volcano, Stolz, 1985) and to change the nomenclature of the rock sequence from olivine basalt–hawaiite–mugearite–benmoreite–trachyte–rhyolite to olivine basalt–hawaiite–trachyandesite–tristanite–trachyte–rhyolite sequence. The work discussed below is relevant to both types and a distinct separation is not made here.

For the ocean island silica-saturated alkalic suites, where no partial melting of continental crust can be called upon, there is a strong consensus for ascribing the dominant mechanism for generating the silica-saturated alkalic trends to crystal fractionation (Bowen, 1937; Macdonald, 1974; Mungall & Martin, 1995; Kar *et al.*,

*Corresponding author. E-mail: Hanna.Nekvasil@sunysb.edu.

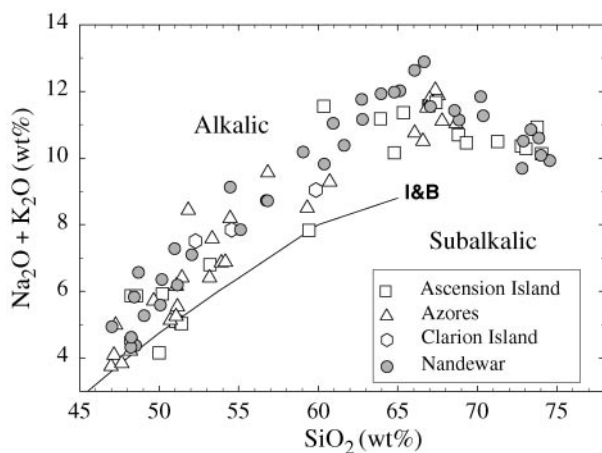


Fig. 1. Variation of total alkalis with silica in bulk compositions of lavas of silica-saturated alkalic suites of Terceira, Azores (Schmincke, 1973; Self & Gunn, 1976; White *et al.*, 1979; Mungall & Martin, 1995), Clarion Island, Mexico (Bryan, 1967), Ascension Island (Harris, 1983) and the Nandewar Volcano, N.S.W., Australia (Abbott, 1969; Stolz, 1985). I&B, subalkalic-alkalic boundary of Irvine & Baragar (1971).

1998). It has been proposed that the compositional trends arise from early crystallization of plagioclase, titanite, and olivine in an olivine basalt, followed by fractionation of an olivine-free magnetite-bearing assemblage, a fayalite, ferroaugite, and alkali feldspar-bearing assemblage and, finally, a kaersutite-bearing assemblage (White *et al.*, 1979; Harris, 1983; Haase *et al.*, 1997). Although crystal fractionation has been called upon by some workers for the continental *hy*-normative alkalic suites (e.g. Abbott, 1969; Barberi *et al.*, 1975; Ewart, 1981; Stolz, 1985), this has generally been limited to describing the possible relationship among intermediate units, leaving the origin of the hawaiite, trachyandesite, and commonly associated rhyolites to other processes such as partial melting of lower crust or lithospheric mantle (Bailey, 1964, 1974; Wright, 1969; Macdonald *et al.*, 1970; Stolz, 1985). It has also been suggested that associated peralkaline felsic rocks may form by a combination of processes involving fractionation as well as compositional changes during volatile exsolution (Macdonald, 1987; Upton & Emeleus, 1987). However, the common thread of crystal fractionation remains dominant even in proposed multi-process origins for these suites.

Experimental investigation of alkalic suites has given rise to voluminous literature on crystal-liquid equilibria in both synthetic and natural silica-undersaturated alkalic melts. Much less is known about phase equilibria of the silica-saturated alkalic systems. [In view of the relationship between ferrous:ferric ratio and calculated normative *nepheline* (*ne*) content, alkalic suites that contain some normative *ne* (i.e. <2 wt %) at an atomic $\text{Fe}^{2+}/(\text{Fe}^{2+} + \text{Fe}^{3+})$ ratio of unity but are not *ne*-normative at ferrous:ferric ratios of 0.8 will be included in the following discussion.] The experimental work described

here was undertaken with two primary interrelated objectives. First, it was designed to provide insights into fractionation paths of natural *hy*-normative alkalic basalt that can be generalized to all silica-saturated alkalic suites. Second, it was designed to provide a foundation that can be used to evaluate the detailed magmatic history of natural suites from individual complexes. Rocks from the Nandewar shield volcano in New South Wales, Australia, were used for this study because of the full spectrum of typical alkalic compositions spanned, the availability of hand samples, and the extensive field, petrographic and analytical work that has already been carried out on the suite (Abbott, 1969; Stolz, 1985, 1986). The starting materials were mainly powders made directly from samples studied petrographically by Abbott (1969) and Stolz (1985). A few additional compositions were synthesized here for this study when hand samples that reasonably matched residual liquid compositions were not available. The compositions of all starting materials are listed in Table 1.

THE NANDEWAR VOLCANO

The Nandewar volcano makes up the Nandewar Mountains of New South Wales, Australia. It is one of several Cenozoic extrusive centers thought to be associated with a mantle plume that impinged on the base of the Australian plate as it moved northwards away from Antarctica (Wellman & McDougall, 1974; Johnson *et al.*, 1989). After an episode of eruption of alkali rhyolite and trachyte (Stipp & McDougall, 1968), the main shield-forming event of this volcano produced lavas of hawaiite, trachyandesite, tristanite, and trachyte compositions (Wellman *et al.*, 1969; Wellman & McDougall, 1974). The volcanic pile was intruded soon thereafter by dikes and plugs of peralkaline trachyte, comendite, and metaluminous rhyolite (Abbott, 1969; Stolz, 1985).

The major element chemistry of the Nandewar units is typical of other silica-saturated alkalic series (Figs 1 and 2). Trace element abundances are also typical, showing marked increases in Li, Rb, Y, Zr, Nb, Hf, Ta, U and Th, and depletion in Cr, Ni, V, Sr and Ba, with increasing silica (Stolz, 1985). Rare earth elements (REE) increase moderately from hawaiite toward trachyte with negligible change in the light REE to heavy REE (LREE/HREE) ratios. However, the systematic variation in abundances of Li, Y, Zr, Zn and, to a lesser extent, Nb and Th, changes abruptly in the peralkaline trachyte; this behavior is mirrored in the comendite and metaluminous rhyolite. Rhyolites are enriched in HREE relative to trachytes. Their LREE abundances are variable, with some exhibiting strong enrichment in LREE and others lower LREE contents than several trachytes.

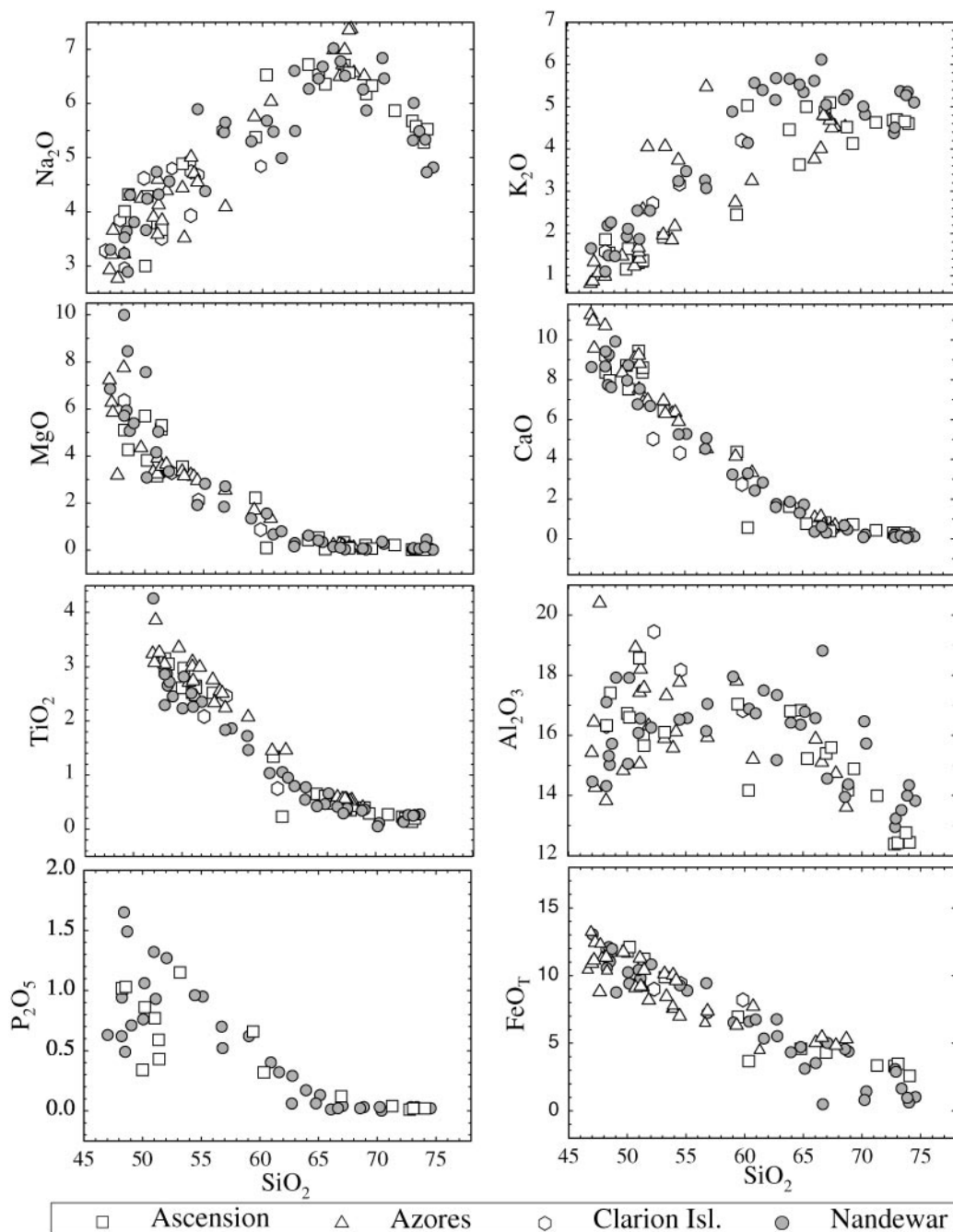


Fig. 2. Variation of major oxides with silica in the lavas plotted in Fig. 1. Sources of data are as in Fig. 1.

Using assimilation–fractional crystallization (AFC) modeling, Stolz (1985) assessed the possibility of generating the mafic and intermediate members of the Nandewar suite by crystal fractionation of the associated hawaiite. He used compositions of the phenocrysts observed in hand samples to simulate the fractionating assemblages. Using the observed mineral assemblages, Stolz (1985) was able to produce the trend from trachyandesite to

trachyte, but he was not able to generate the trachyandesite from the hawaiite or the most silicic rocks from the trachyte through these calculations. The difficulty in computationally deriving trachyandesite from the hawaiite stems from the presence of a significant amount of crystalline plagioclase in the hawaiite hand samples. Plagioclase in the crystalline assemblage inhibits the strong increase in alkalis relative to silica that marks the

Table 1: Compositions of starting materials A–E (wt %)

| Sample: | A | B | C | D | E |
|-----------------------------------|----------|----------------|----------------|-----------------|-----------|
| | Hawaiite | Trachyandesite | Alkali syenite | Felsic trachyte | Mugearite |
| | 49000* | 49005* | 15799† | | 15795† |
| Type: | Natural | Natural | Natural | Synthetic | Natural |
| SiO ₂ | 46.99 | 47.06 | 56.42 | 66.18 | 53.36 |
| TiO ₂ | 2.65 | 2.79 | 1.46 | 0.41 | 1.80 |
| Al ₂ O ₃ | 14.55 | 14.88 | 16.93 | 17.14 | 16.04 |
| Fe ₂ O ₃ | 1.77 | 3.17 | 3.50 | 0.61 | 5.71 |
| FeO | 8.90 | 8.58 | 4.07 | 3.11 | 3.73 |
| MnO | 0.13 | 0.15 | 0.09 | 0.07 | 0.2 |
| MgO | 8.18 | 5.76 | 2.71 | 0.37 | 2.73 |
| CaO | 8.97 | 7.51 | 5.06 | 1.76 | 5.10 |
| Na ₂ O | 2.80 | 3.54 | 5.65 | 5.79 | 4.24 |
| K ₂ O | 1.43 | 2.13 | 3.07 | 4.37 | 3.36 |
| P ₂ O ₅ | 0.47 | 1.60 | 0.52 | 0.19 | 0.92 |
| H ₂ O ⁺ | 2.03 | 1.84 | 0.87 | 1.73 | |
| H ₂ O ⁻ | 0.83 | 0.87 | | | |
| Total | 99.70 | 99.34 | 100.73 | 100.00 | 99.41 |
| Bulk H ₂ O wt % (FTIR) | 2.0 | 2.3 | 1.4 | 0.1 | 4.3 |

*Stolz (1985). †Abbott (1969).

difference between the hawaiite and trachyandesite (Fig. 2). Furthermore, unless the amount of olivine exceeded the amount of plagioclase and clinopyroxene in the fractionating assemblage, the silica content of the evolving melt would decrease rather than remain essentially constant. Stolz (1985) ascribed the computational difficulty in deriving trachyandesite from hawaiite to different source materials for these units. However, this difficulty may instead reflect an incorrect choice of fractionating assemblage.

If fractionation occurred at depths greater than that at which the observed assemblage was in equilibrium, then a difference in assemblage could result in very different liquid lines of descent. The higher-pressure assemblages could give rise by fractionation to liquid compositions that represent the observed bulk lava compositions. These ascending liquids could pond before reaching the surface and crystallize a low-pressure assemblage. As long as this low-pressure assemblage was not involved in any new fractionation step, the high-pressure liquid line of descent would be preserved in the bulk compositions, even if crystalline evidence of the fractionation assemblage is scant. That some portion of the crystallization history of these magmas does occur at pressures significantly higher than the subvolcanic region is evidenced by the presence of tschermakitic Ca-rich pyroxene and aluminous bronzite phenocrysts in trachyandesite. These crystals

yield pressures of 6–8 kbar (Ewart, 1981; Stolz, 1985) and coexist with low-Al pyroxenes, suggesting a polybaric history. Discontinuous feldspar compositions in the mafic rocks are also consistent with a polybaric history (Nekvasil *et al.*, 2000). The presence of higher-pressure phases associated with a low-pressure assemblage is common to many alkalic provinces (e.g. Ghorbani & Middlemost, 2000) and suggests that more than one stage of ponding may be the rule in alkalic provinces.

The phase equilibrium experiments described below were designed to explore the possibility of fractionation control on the compositional diversity of bulk compositions of units within silica-saturated alkalic suites and to constrain the depths and water contents at which such fractionation could give rise to the bulk lava compositions characteristic of these suites. In addition, they were designed to constrain conditions under which the observed mineral assemblages in the natural rock units could have been produced.

EXPERIMENTAL METHODS

Experimental strategy

In nature, crystal fractionation occurs when melt loses the contact needed with the crystalline assemblage to continually re-establish equilibrium during cooling. This

process can occur in a variety of ways, from gravitational settling or sidewall crystallization to filter pressing, and, in all cases, is likely to be incremental rather than continuous. The experiments described below simulate an incremental fractionation path in which melt evolves by equilibrium crystallization punctuated by periodic removal of crystals. This process has been simulated by first crystallizing a selected bulk composition at several temperatures. Then, once a residual melt composition is found that is similar to a natural lava of the suite, the starting material is switched so that the new sample becomes the bulk composition for the next set of equilibrium experiments, and so forth.

Oxygen fugacity

The importance of externally imposed f_{O_2} in dictating phase equilibria in Fe-bearing systems has been well recognized in the literature. Although the range of f_{O_2} in which alkalic magmas crystallize is not well known, it has been suggested that it extends from the fayalite–magnetite–quartz buffer (FMQ) to significantly below [e.g. about 2 log units below FMQ for some pantellerites (Carmichael & Ghiorso, 1990)]. There is little evidence, however, that a crystalline buffering assemblage is present in these silica-saturated alkalic systems over a significant range of temperatures. Thus, f_{O_2} variation during crystallization in natural systems may differ significantly from any specific oxygen buffer curve, depending upon the partitioning of ferrous and ferric Fe between crystals and melt. In the experiments discussed below, the f_{O_2} was not directly buffered. Efforts were made, however, not to dramatically change the f_{O_2} of the natural assemblage by, for example, oxidizing the sample during drying. Adsorbed water was driven off by drying at 175°C under vacuum; structural water was driven off at 800°C under vacuum and in the presence of an Fe^o oxygen getter which was at ~600°C. Use of graphite capsules for the piston-cylinder experiments constrained the f_{O_2} to be at or below the GCO [graphite–(C–O fluid)] buffer. (Use of these capsules had the additional benefit of avoiding Fe loss to metal capsules.) Whenever an assemblage existed in the piston-cylinder experimental run products that permitted the f_{O_2} to be computed using the QUIF method of Andersen *et al.* (1993), the results for the 9.3 and 4.3 kbar experiments yielded f_{O_2} values between 1.5 and 0.5 log unit below FMQ.

For the silica-tube experiments at 0 kbar, care was also taken not to oxidize the sample during drying at 800°C. Additionally, Fe^o was added to the sample to prevent oxidation of the melt by loss of iron from FeO to the Au₈₀Pd₂₀ capsule walls. The computed f_{O_2} varied between 1 and 2 log units above FMQ for 0 kbar experiments on natural rocks and between 0.5 and 1 log units above FMQ for the synthetic mix.

Water content

The importance of water in dictating phase equilibria has also been long recognized. For this reason, water content was a constrained variable in all experiments. Continuity of fractionation paths with respect to water content across fractionation steps required that the water content at each fractionation step be measured and that of the new starting material adjusted to that of the residual glass of the previous experiment. In practice, this was difficult and resulted in some deviation from a continuous path.

Structurally bound water in the natural samples was used instead of added water as the starting point for NVA (no-volatiles-added) experiments. It is unlikely that this water represents entirely magmatic water, but this water content does provide phase equilibrium constraints for conditions of 'high' water content. Furthermore, use of these samples was highly convenient in that this water was readily retained by the sample in the graphite capsules. For NVA experiments, rock powders were dried under vacuum at 175°C to remove adsorbed water. Additional experiments were conducted at water contents other than that of the natural rock. In these cases, H₂O was added to undried or dried rock powders (volatiles added, or VA experiments), and the mixture was melted in graphite-lined Pt capsules at 10 kbar. The hydrous glass produced was used as the new starting material for phase equilibrium experiments. This method of adding water was necessitated by the observation that water added directly to a graphite capsule was commonly lost by the time the melting temperature was attained.

Some experiments were also performed with dried powders of the natural samples (DRY). These samples were dried under vacuum at 800°C for 20 min in the presence of Fe^o sponge. However, it proved difficult to achieve precisely the same water content during the drying process. Because, at low bulk water contents, small differences in bulk water content have significant effects on liquid lines of descent, micro-FTIR (Fourier Transform Infrared) analysis of run products proved imperative for each DRY experiment in order to systematize these effects.

The question of equilibrium

All phase equilibrium experiments were crystallization experiments in which the starting material was heated above the liquidus at 1250°C for 6 h before the temperature was dropped to the desired value. Because of the differences in mineral assemblage between the natural rocks and the high-pressure experimental products, crystallization experiments cannot be reversed by partial melting of the natural samples with their low-pressure assemblages without significant potential for metastable effects. Instead, the likelihood of an equilibrium

assemblage was evaluated by checking for consistency in phase compositions in successively lower-temperature experiments, computational testing by using QUIF (Andersen *et al.* 1993) to evaluate the possibility of equilibrium between the ferromagnesian minerals, and checking for zoning in feldspars and pyroxenes. Only the low-temperature experiments containing <10 vol. % liquid commonly showed feldspar zoning.

Experimental details

Starting materials

The natural rock powders (Table 1) used for most experiments were from samples kindly provided by the University of New England, Armidale, Australia, and The Australian National University. Late-stage liquids for which natural samples were not available were synthesized by a mixture of SiO₂, TiO₂, Al₂O₃, Fe₂O₃, Fe^o sponge, MnO, MgO, CaSiO₃, NaAlSi₃O₈ gel, KAlSi₃O₈ gel, and Ca₃(PO₄)₂ that was homogenized by grinding and then heated at 800°C in vacuum and in the presence of an oxygen getter. The ferrous/Fe_T ratio for the synthetic mix was chosen to be 0.85. The final composition of the mix was verified by electron microprobe analysis after fusion.

Piston-cylinder experiments

Extra-dense BaCO₃ sleeves with exterior Pb liners were used for all piston-cylinder experiments. Ba contamination of the sample is a possibility with these sleeves; however, random Ba analyses of experimental glasses indicated that this was very rare and limited to samples where fracturing of the graphite capsule was evident in thin section. Graphite furnaces were inserted into the sleeves. Graphite capsules with lids, machined for a tight fit, and mullite spacers were placed inside the furnaces. An alumina disk separated the thermocouple from the graphite capsule. Temperature was monitored with a Pt–Pt₉₀Rh₁₀ thermocouple. Temperature calibration for the assembly yielded a 14°C positive gradient from the thermocouple to the center of the capsule. Temperatures reported are those at the hot spot. Pressure calibration of the cells using the reaction Mg-cordierite = sapphirine + quartz (Newton *et al.*, 1974) at 7 kbar yielded ~0.7 kbar negative correction. Although this correction is probably somewhat pressure sensitive, it was assumed here that this pressure correction is appropriate for all pressures within the range 3.5–9.3 kbar.

Experiments at 0 kbar

Silica-tube experiments were conducted in Pt-wound quench furnaces. For these experiments, the powdered Fe^o-enriched sample was placed in a crimped Au₈₀Pd₂₀

tube, which in turn was placed in a silica glass tube. The tube was evacuated and the sample dried at 800°C in the presence of an Fe^o oxygen getter. After sealing, the tube was hung by a Pt wire in the furnace and gradually lowered to the hot spot. The sample was quenched in water. The combined thermal gradient and thermocouple uncertainty is probably no more than 5°C.

Analysis of experimental run products

Electron microprobe analysis was used to obtain the abundances of the major elements of all phases. For Na analysis of glasses, the beam current was reduced to 2 nA (for analyses conducted at the American Museum of Natural History) or 4 nA (for analyses conducted at SUNY Stony Brook) and the largest possible beam size was used. For highly evolved hydrous glasses, loss of both Na and K during analysis was evidenced by calculated normative corundum (*co*). The amount of excess alumina was reduced when a zero-time correction was implemented. Additional excess *co* was removed computationally from glass analyses by the addition of Na₂O to each analysis (prior to renormalization) just to the point when all normative *co* was converted to albite, not beyond. The assignment of this excess alumina to Na loss may result in slight overestimates of Na₂O contents in liquid and underestimates of K₂O. However, mass balance least-squares analysis showed a major improvement in sodium mass balance after this correction. In the rare cases when sodium excess resulted from this correction procedure (as noted by mass balance constraints), then the added Na₂O was reduced and K₂O added for better mass balance. Feldspar data were checked for stoichiometry and Na was corrected if needed. All pyroxene, olivine and oxide data were projected through QUIF via the method of Andersen *et al.* (1993). Mass balance calculations were conducted for all crystalline phase bearing run products using the software IgPet for Windows (Carr, 2000). Only mineral analyses that yielded good stoichiometries and phase compositions that yielded sums of the squares of the residuals of <0.5 were accepted and tabulated in this paper.

Water contents of selected experimental glasses were determined by IR spectroscopic measurements conducted in transmittance mode using a Nicolet 20SXB FTIR spectrometer attached to a Spectra Tech IR Plan microscope at the American Museum of Natural History. Total dissolved water concentrations in doubly polished glass or glass + crystal wafers were determined from the intensity of the broad band at 3570 cm⁻¹. Approximately 1024 scans were performed for each IR spectrum acquired. Thicknesses of the wafers were measured using a Mitutoyo digimatic indicator. Total water concentrations were calculated via the method of Dixon *et al.* (1995) using a molar absorptivity of 62 L/mol cm

(Mandeville *et al.*, 2002) and calculated glass densities (Dixon *et al.*, 1995). A more detailed discussion of the technique used has been given by Mandeville *et al.* (2002).

Water content analysis of the experimental run products was commonly less precise than considered usual for the technique. This problem was linked to the low precision of thickness measurements caused by the use of very thin wafers of polyphase assemblages—a use made necessary to ensure IR beam transmission through a single phase. The thickness uncertainty overwhelmed both the accuracy of the absorption coefficient used and the calculated glass density. The net uncertainty of the reported water contents may be as much as 10 relative wt %.

EXPERIMENTAL RESULTS

The experiments yielded subhedral crystals and glass, with only sporadic evidence of zoning. Textural evidence for fluid saturation was rare and suggests the possibility of fluid loss through the graphite capsule. Glass water contents, where analyzed in a polyphase assemblage, suggest, however, that dissolved water prior to fluid saturation was retained during the experiment and quench. Glass was chemically homogeneous except for samples in which <5% glass remained.

Phase relations at 9.3 kbar

'High' water contents

Phase relations at 9.3 kbar for 'high' water contents were determined along an incremental fractionation path that spanned the entire compositional range from hawaiite (**A**; sample 49000) through trachyandesite (**B**; sample 49005) and alkali syenite (**C***, sample 15799 with 4 wt % H₂O) to mafic rhyolite with 5.1% H₂O (**D**). These rocks represent the starting compositions for each incremental fractionation step along the path.

Figures 3a and 4 and Table 2 show the major element compositions of liquids produced by crystallization of each sample. An initial strong increase in alkali content occurs in liquids evolving from hawaiite (**A**) with little change in silica content, induced by the near-liquidus crystallization of a clinopyroxene-dominated, clinopyroxene + olivine assemblage. In this way, mildly alkalic parental liquids can produce more strongly alkalic residual liquids during crystallization. The strong increase in alkalis with silica is moderated once kaersutite appears, and the silica content of the evolving liquid increases more rapidly. By 50% crystallinity of hawaiite **A** the liquid has evolved through **B** to a trachytic composition. Trachytic liquid with 4 wt % bulk water (**C***) evolves to mafic rhyolite (Fig. 4). However, because the alkali syenite **C*** lies compositionally slightly offset from the **A–B** evolutionary path with higher CaO and Na₂O contents

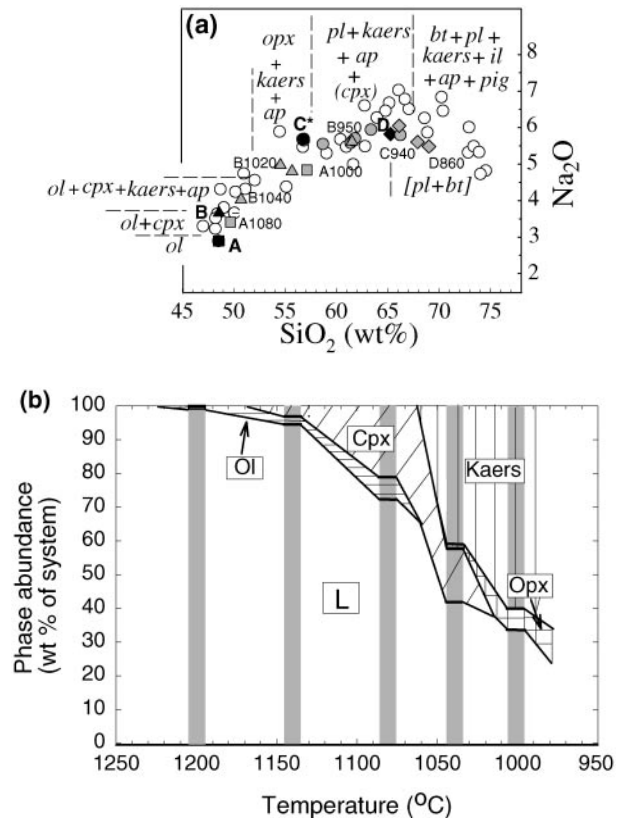


Fig. 3. (a) Variation in Na₂O vs silica in residual liquids along the stepwise fractionation path **A–D** at 9.3 kbar. Bulk compositions, **A–D**, are given in Table 1. Temperatures of select experiments are indicated by labels with bulk composition followed by temperature (in °C) of the experiment (e.g. A1080). Phases crystallizing along the path are indicated as well as the segment of the path along which the assemblage is found (dashed boundaries). Phase abbreviations are as in Table 2. The assemblage crystallizing from residual liquids of **B** contains no clinopyroxene in this region [indicated by (cpx)], but clinopyroxene is present in the same temperature range for liquids emanating from **C***. Square brackets indicate the mineral assemblage for liquids emanating from **D**. ○, bulk compositions from the Nandewar volcano. (b) Variation in phase abundances for bulk composition **A** (NVA), showing the early dominance of clinopyroxene in the assemblage, and absence of plagioclase. Phase abbreviations are as in Table 2.

and lower K₂O contents (Fig. 4), its evolutionary path is also slightly offset from the **A–B** path. This difference is further reflected in the early stabilization of a high-calcium pyroxene rather than the orthopyroxene produced in **A** and **B**. However, as in **A** and **B**, kaersutite remains volumetrically the most abundant crystalline phase (at the intermediate stage of evolution) until the late stages when plagioclase abundance increases markedly and the liquid becomes rhyolitic.

For composition **C***, mafic rhyolite is produced by crystallization of kaersutite, plagioclase and biotite at low temperatures. The synthetic version of the residual liquid of **C*** at 940°C, **D**, however, crystallizes an amphibole-free plagioclase + biotite assemblage at 900°C as the

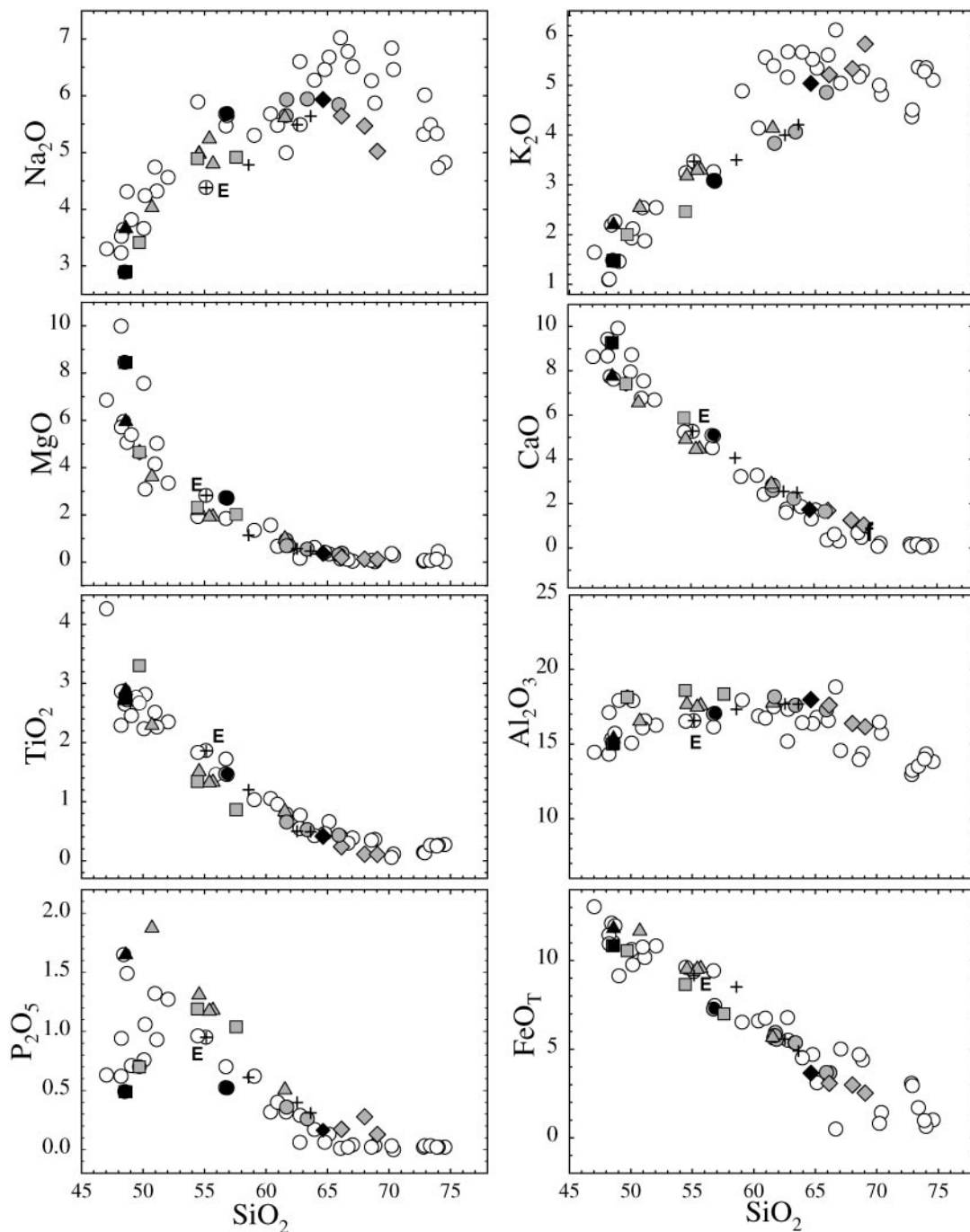


Fig. 4. Variation in major oxides of liquids along the paths of Fig. 3. Symbols are as in Fig. 3. The liquid line of descent of **E** is shown by the series of +.

liquid evolves to mafic rhyolite. This difference in assemblage may arise from either or both of the two primary differences between the synthetic and residual liquids. It may reflect the higher K_2O content of the synthetic derivative relative to the residual liquid of **C*** at $940^\circ C$, or it may reflect a discontinuity in water content. The water content of **C*** at $940^\circ C$ could not be measured

readily by FTIR because of the abundance and distribution of the crystals; therefore, the selected value of 5.1 wt % for **D** may be lower than that of the residual liquid of **C*** at $940^\circ C$. This is consistent with the stability of Ti-rich biotite (Table 3) in **D**. As has been noted by others (e.g. Zhou, 1994), we have observed that high-Ti biotite routinely appears at lower water contents than

Table 2: Representative residual liquid compositions and phase assemblages along the path A–B–C*–D at 9.3 kbar of Figs 3 and 4

| Starting material: | A | A | A | A | A | A |
|------------------------------------|-----------|-------------------------------|--------------|------------------------|---------------------------------|------------------------------|
| Bulk water content (wt %): | NVA (2-3) | NVA (2-3) | NVA (2-3) | NVA (2-3) | NVA (2-3) | NVA (2-3) |
| Equilibration temperature (°C): | 1250 | 1200 | 1130 | 1080 | 1040 | 1000 |
| SiO ₂ | 46.99 | 47.16 | 47.2 | 47.25 | 52.25 | 56.17 |
| TiO ₂ | 2.65 | 2.66 | 2.69 | 3.14 | 1.24 | 0.84 |
| Al ₂ O ₃ | 14.55 | 14.6 | 14.88 | 17.24 | 17.80 | 17.91 |
| FeO _T | 10.49 | 10.53 | 10.69 | 10.04 | 8.29 | 6.82 |
| MnO | 0.13 | 0.13 | 0.14 | 0.10 | 0.26 | 0.10 |
| MgO | 8.18 | 8.21 | 7.27 | 4.42 | 2.53 | 1.97 |
| CaO | 8.97 | 9.00 | 8.91 | 7.05 | 5.63 | 5.38 |
| Na ₂ O | 2.80 | 2.81 | 2.86 | 3.24 | 3.79 (4.6) | 3.39 (4.8) |
| K ₂ O | 1.43 | 1.44 | 1.36 | 1.90 | 2.42 | 2.45 |
| P ₂ O ₅ | 0.47 | 0.47 | 0.50 | 0.67 | 1.10 | 1.01 |
| Total | 96.66 | 97.01 | 96.50 | 95.05 | 95.33 | 96.04 |
| Molar Mg no. | 62 | 62 | 59 | 48 | 39 | 37 |
| Phases | L | Ol + L | Ol + Cpx + L | Ol + Cpx + L | Cpx + Opx + Kaers + Ap + L | Opx + Kaers + Ap + L |
| Water in residual glass (wt %) | 2.3 | 2.4 | | 3.1 | | |
| Crystallinity (wt %); s.s.r. < 0.4 | 0 | < 1% Ol | 5 (3% Cpx) | 27 (21% Cpx) | 58 (16% Cpx; 41% Kaers; 1% Opx) | 62 (56% Kaers; 6% Opx) |
| Starting material: | B | B | B | B | B | B |
| Bulk water content (wt %): | NVA (2) | NVA (2) | NVA (2) | NVA (2) | NVA (2) | NVA (2) |
| Equilibration temperature (°C): | 1250 | 1040 | 1020 | 1000 | 950 | 950 |
| SiO ₂ | 47.06 | 48.09 | | 52.54 | 52.84 | 59.91 |
| TiO ₂ | 2.79 | 2.18 | | 1.45 | 1.26 | 0.81 |
| Al ₂ O ₃ | 14.88 | 15.68 | | 17.00 | 16.68 | 17.29 |
| FeO _T | 11.43 | 11.06 | | 9.18 | 9.08 | 5.52 |
| MnO | 0.15 | 0.15 | | 0.17 | 0.15 | 0.08 |
| MgO | 5.76 | 3.43 | | 2.11 | 1.82 | 0.97 |
| CaO | 7.51 | 6.22 | | 4.73 | 4.25 | 2.80 |
| Na ₂ O | 3.54 | 3.82 | | 4.79 | 4.56 | 4.17 (5.47) |
| K ₂ O | 2.13 | 2.42 | | 3.06 | 3.14 | 4.03 |
| P ₂ O ₅ | 1.6 | 1.78 | | 1.26 | 1.12 | 0.49 |
| Total | 96.85 | 94.83 | | 96.29 | 94.90 | 96.07 |
| Molar Mg no. | 51 | 39 | | 33 | 30 | 25 |
| Phases | L | Ol + Cpx + Kaers + Ap + L | | Opx + Kaers + Ap + L | Opx + Kaers + Ap + L | Kaers + Il + Pl + Ap + L |
| Water in residual glass (wt %) | 2 | | | 3.3 | | |
| Crystallinity (wt %); s.s.r. < 0.4 | 0 | 23 (20% Kaers; 2% Cpx; 1% Ol) | | 38 (31% Kaers; 5% Opx) | 46 (40% Kaers; 4% Opx) | 63 (50% Kaers; 6% Il; 4% Pl) |

Table 2: continued

| | | | | |
|-----------------------------------|-------------|---------------------------------------|-------------------------------|-------------------------------|
| Starting material: | C* | C* | C* | C* |
| Bulk water content (wt %): | 4 | 4 | 4 | 4 |
| Equilibration temperature (°C): | 1250 | 980 | 960 | 940 |
| SiO ₂ | 56.42 | 58.58 | 60.67 | 62.21 |
| TiO ₂ | 1.46 | 0.62 | 0.50 | 0.41 |
| Al ₂ O ₃ | 16.93 | 17.25 | 16.85 | 16.32 |
| FeO _T | 7.22 | 5.47 | 5.13 | 3.47 |
| MnO | 0.09 | 0.11 | 0.11 | 0.05 |
| MgO | 2.71 | 0.66 | 0.52 | 0.29 |
| CaO | 5.06 | 2.67 | 2.13 | 1.56 |
| Na ₂ O | 5.65 | 5.06 (5.63) | 4.96 (5.69) | 5.30 (5.51) |
| K ₂ O | 3.07 | 3.65 | 3.89 | 4.58 |
| P ₂ O ₅ | 0.52 | 0.34 | 0.25 | 0.12 |
| Total | 99.13 | 94.38 | 95.02 | 94.31 |
| Molar Mg no. | 44 | 20 | 17 | 15 |
| Phases | L | Cpx + Kaers + Pl + Ap + tr.II | Kaers + Pl + Ap + tr.II + L | Kaers + Pl + Ap + tr.II + L |
| Water in residual glass (wt %) | 4 | | | |
| Crystallinity (wt %); s.s.r. <0.4 | 0 | 32 (19% Kaers; 11% Pl; 2% Cpx; 1% Ap) | 40 (23% Kaers; 14% Pl; 3% Ap) | 66 (29% Kaers; 36% Pl; 2% Ap) |
| Starting material: | D | D | D | D |
| Bulk water content (wt %): | 5 | 5 | 5 | 5 |
| Equilibration temperature (°C): | 940 | 900 | 880 | 860 |
| SiO ₂ | 63.94 | 62.42 | 64.67 | 63.99 |
| TiO ₂ | 0.41 | 0.22 | 0.11 | 0.12 |
| Al ₂ O ₃ | 17.79 | 16.63 | 15.58 | 15.08 |
| FeO _T | 3.62 | 2.90 | 2.84 | 2.31 |
| MnO | 0.06 | 0.03 | 0.03 | 0.03 |
| MgO | 0.37 | 0.18 | 0.12 | 0.10 |
| CaO | 1.72 | 1.60 | 1.19 | 1.04 |
| Na ₂ O | 4.60 (5.87) | 5.23 (5.33) | 4.8 (5.2) | 4.68 (4.77) |
| K ₂ O | 4.99 | 4.92 | 5.07 | 5.21 |
| P ₂ O ₅ | 0.16 | 0.16 | 0.27 | 0.07 |
| Total | 97.66 | 94.29 | 94.65 | 92.71 |
| Molar Mg no. | 18 | 11 | 8 | 8 |
| Phases | L + Pl | Bt + Pl + L | Pl + Bt + L | Pl + Bt + L |
| Water in residual glass (wt %) | 5.1 | | | |
| Crystallinity (wt %); s.s.r. <0.4 | 1 (1% Pl) | 10 (8% Pl) | 25 (20% Pl) | 53 (47% Pl) |

Na values in parenthesis are corundum-corrected values. Crystallinity reported from least-squares calculations and confirmed visually. Percentages of phases are for entire system. s.s.r., sum of the squares of residuals from mass balance least-squares calculation of phase abundances. Phases: Ol, olivine; Cpx, clinopyroxene; L, liquid; Opx, orthopyroxene; Ap, apatite; Kaers, kaersutite; Pl, plagioclase; Il, ilmenite; Bt, biotite.

Table 3: Representative mineral compositions along the path **A–B–C*–D** at 9.3 kbar of Figs 3 and 4

| | | | | | | | | |
|---------------------------------|--|---|--|--------------------------|--|-------------|--|---|
| Starting material: | A | A | A | A | A | A | A | A |
| Bulk water content (wt %): | NVA | NVA | NVA | NVA | NVA | NVA | NVA | NVA |
| Equilibration temperature (°C): | 1200 | 1130 | 1130 | 1080 | 1080 | 1040 | 1040 | 1040 |
| Phase: | olivine | olivine | clinopyroxene | olivine | clinopyroxene | kaersutite | clinopyroxene | orthopyroxene |
| SiO ₂ | 38.92 | 39.22 | 52.03 | 36.81 | 46.9 | 38.99 | 49.94 | 50.27 |
| TiO ₂ | 0.00 | 0.01 | 0.95 | 0.00 | 1.96 | 5.24 | 0.95 | 0.57 |
| Al ₂ O ₃ | 0.00 | 0.00 | 4.08 | 0.05 | 7.17 | 13.83 | 4.57 | 4.61 |
| FeO _T | 17.38 | 18.41 | 6.42 | 25.87 | 9.08 | 12.79 | 12.11 | 19.69 |
| MnO | 0.12 | 0.20 | 0.12 | 0.16 | 0.11 | 0.10 | 0.21 | 0.28 |
| MgO | 43.24 | 42.46 | 18.14 | 37.39 | 14.23 | 11.47 | 14.17 | 20.67 |
| CaO | 0.17 | 0.20 | 17.8 | 0.25 | 18.07 | 9.52 | 15.77 | 2.13 |
| Na ₂ O | 0.11 | 0.00 | 0.43 | 0.03 | 0.55 | 2.45 | 0.42 | 0.05 |
| K ₂ O | 0.01 | 0.01 | 0.00 | 0.01 | 0.02 | 0.93 | 0.03 | 0.01 |
| P ₂ O ₅ | 0.06 | 0.15 | 0.03 | 0.00 | 0.27 | 0.04 | 0.02 | 0.00 |
| Total | 100.01 | 100.66 | 100.00 | 100.57 | 98.36 | 95.36 | 98.19 | 98.28 |
| Phase comp. (mol %) | Fo ₈₂ Fa ₁₈ (0.23) | Fo ₈₀ Fa ₂₀ (0.27) | En ₅₇ Wo ₃₃ Fs ₁₀ | Fo ₇₂ Fa(0.3) | En ₅₄ Wo ₃₂ Fs ₁₄ | | En ₄₈ Wo ₂₈ Fs ₂₄ | En ₆₂ Wo ₅ Fs ₃₃ |
| Starting material: | A | A | B | B | B | B | B | B |
| Bulk water content (wt %): | NVA | NVA | NVA | NVA | NVA | NVA | NVA | NVA |
| Equilibration temperature (°C): | 1000 | 1000 | 1020 | 1020 | 1000 | 1000 | 950 | 950 |
| Phase: | kaersutite | orthopyroxene | orthopyroxene | kaersutite | orthopyroxene | kaersutite | plagioclase | kaersutite |
| SiO ₂ | 41.86 | 51.4 | 48.49 | 39.62 | 50.37 | 39.8 | 59.13 | 37.96 |
| TiO ₂ | 4.16 | 0.34 | 0.33 | 6.15 | 0.61 | 5.25 | 0.07 | 5.56 |
| Al ₂ O ₃ | 13.95 | 2.39 | 5.31 | 13.53 | 4.35 | 13.20 | 24.81 | 14.55 |
| FeO _T | 12.56 | 21.74 | 23.00 | 14.58 | 22.28 | 13.67 | 0.36 | 16.89 |
| MnO | 0.15 | 0.30 | 0.51 | 0.16 | 0.38 | 0.17 | 0.00 | 0.18 |
| MgO | 11.71 | 21.16 | 21.03 | 11.74 | 19.72 | 9.94 | 0.01 | 9.09 |
| CaO | 10.38 | 1.70 | 1.66 | 9.45 | 1.90 | 9.95 | 6.25 | 9.12 |
| Na ₂ O | 2.46 | 0.06 | 0.00 | 2.50 | 0.11 | 2.39 | 6.87 | 2.64 |
| K ₂ O | 0.89 | 0.02 | 0.07 | 0.83 | 0.01 | 1.08 | 1.19 | 0.74 |
| P ₂ O ₅ | 0.10 | 0.03 | 0.00 | 0.16 | 0.01 | 0.05 | 0.00 | 0.40 |
| Total | 98.22 | 99.14 | 100.40 | 98.72 | 99.74 | 95.50 | 98.69 | 97.13 |
| Phase comp. (mol %) | | En ₆₁ Wo ₄ Fs ₃₅ | En ₆₅ Wo ₄ Fs ₃₁ | | En ₅₉ Wo ₄ Fs ₃₇ | | An ₃₀ Ab ₆₃ Or ₇ | |

kaersutite. Further experimentation along the liquid line of descent of **D** to determine if the more felsic units of the natural suites could be produced was not conducted here for three primary reasons. First, after ~60% crystallinity, the experimental run products showed great crystal dispersion, making analysis of hydrous alkali-rich interstitial glass difficult; second, increasing degrees of feldspar zoning cast increasing doubt on the attainment of equilibrium. Finally, the well-recognized halogen enrichment in late-stage liquids of the silica-saturated suites suggests that the low-F and -Cl experimental conditions do not reflect natural conditions for the felsic units.

The trend defined by the natural Nandewar magmas is broad because of the scatter among units (Fig. 1). Retention of the main liquid line of descent by magmas that lie on the periphery of the primary trend of bulk compositions was ascertained by using a glassy mugearite sample (**E**). Because this sample lies on the low-Na side (Table 1) of the trend, when considered along with the alkali syenite sample 15799 (**C***) (which lies on the high-Na side of the trend of liquids derived from 49005) the scatter is effectively bracketed. Glass **E** already contains about 4 wt % water and all experiments on this sample were NVA. After early clinopyroxene + biotite, a Ba-biotite + kaersutite

Table 3: continued

| | | | | | | | |
|---------------------------------|--|---|--|---|--|--|------------|
| Starting material: | C* | C* | C* | C* | C* | C* | C* |
| Bulk water content (wt %): | 4 | 4 | 4 | 4 | 4 | 4 | 4 |
| Equilibration temperature (°C): | 980 | 980 | 980 | 960 | 960 | 940 | 940 |
| Phase: | clinopyroxene | plagioclase | kaersutite | plagioclase | kaersutite | plagioclase | kaersutite |
| SiO ₂ | 48.84 | 59.84 | 38.49 | 60.55 | 39.45 | 61.86 | 38.62 |
| TiO ₂ | 1.15 | 0.15 | 6.44 | 0.00 | 5.31 | 0.01 | 4.72 |
| Al ₂ O ₃ | 4.40 | 23.75 | 12.88 | 23.80 | 13.12 | 22.88 | 13.07 |
| FeO _T | 15.14 | 0.41 | 17.56 | 0.28 | 18.43 | 0.27 | 19.45 |
| MnO | 0.36 | 0.01 | 0.29 | 0.00 | 0.30 | 0.00 | 0.30 |
| MgO | 9.59 | 0.01 | 7.74 | 0.01 | 7.77 | 0.00 | 6.68 |
| CaO | 18.43 | 5.38 | 10.34 | 5.01 | 10.44 | 4.17 | 9.64 |
| Na ₂ O | 0.77 | 7.60 | 2.40 | 7.89 | 2.83 | 7.96 | 2.76 |
| K ₂ O | 0.08 | 1.01 | 1.03 | 1.24 | 1.06 | 1.63 | 0.94 |
| P ₂ O ₅ | 0.07 | 0.04 | 0.12 | 0.01 | 0.09 | 0.00 | 0.19 |
| Total | 98.83 | 98.20 | 97.29 | 98.79 | 98.80 | 98.78 | 96.36 |
| Phase comp. (mol %) | En ₃₄ Wo ₃₇ Fs ₂₉ | An ₂₆ Ab ₆₈ Or ₆ | | An ₂₄ Ab ₆₉ Or ₇ | | An ₂₀ Ab ₇₀ Or ₁₀ | |
| Starting material: | D | D | D | D | D | D | D |
| Bulk water content (wt %): | 5 | 5 | 5 | 5 | 5 | 5 | 5 |
| Equilibration temperature (°C): | 900 | 900 | 880 | 880 | 860 | 860 | 860 |
| Phase: | plagioclase | biotite | plagioclase | biotite | plagioclase | biotite | biotite |
| SiO ₂ | 63.52 | 34.07 | 63.69 | 38.58 | 63.59 | 37.15 | |
| TiO ₂ | 0.00 | 5.22 | 0.00 | 5.02 | 0.00 | 4.32 | |
| Al ₂ O ₃ | 22.11 | 15.12 | 22.63 | 15.35 | 22.90 | 15.14 | |
| FeO _T | 0.14 | 23.87 | 0.16 | 24.15 | 0.16 | 26.67 | |
| MnO | 0.00 | 0.12 | 0.00 | 0.16 | 0.00 | 0.22 | |
| MgO | 0.00 | 6.09 | 0.01 | 3.85 | 0.00 | 4.37 | |
| CaO | 3.51 | 0.05 | 3.75 | 0.22 | 3.85 | 0.13 | |
| Na ₂ O | 8.66 | 0.73 | 8.35 | 0.92 | 8.09 | 0.74 | |
| K ₂ O | 1.89 | 8.71 | 2.01 | 7.88 | 2.24 | 8.15 | |
| P ₂ O ₅ | 0.00 | 0 | 0.02 | 0.09 | 0.08 | 0.02 | |
| Total | 99.82 | 93.97 | 100.62 | 96.22 | 100.91 | 96.89 | |
| Phase comp. (mol %) | An ₁₉ Ab ₆₈ Or ₁₃ | | An ₁₈ Ab ₆₈ Or ₁₄ | | An ₁₈ Ab ₆₉ Or ₁₃ | | |

Components: Fo, Forsterite; Fa, Fayalite; En, Enstatite; Wo, Wollastonite; Fs, ferrosilite; Ab, albite; An, anorthite; Or, sanidine. Ferromagnesian mineral phase compositions optimized through QUIF. Parenthetical values in olivine analyses are mol % Larnite component. Temperatures in bold indicate change from previous listed temperature.

assemblage crystallizes from **E**. This assemblage is joined close to the solidus by a Ba-rich alkali feldspar. The large amount of Ba in the late-stage biotite and alkali feldspar reflects the high initial Ba content of this sample (Abbott, 1969).

Representative mineral compositions are given in Table 3. Pyroxene and olivine compositions plotted as QUIF projections using the method of Andersen *et al.* (1993) are shown in Fig. 5. Evolution towards decreasing Mg number of the melt is reflected in the Fe enrichment of

the pyroxene and olivine assemblages with falling temperature. The higher CaO content of **C*** relative to the residual liquids of **B** results in the early stabilization of augite.

The compositional relations between feldspar, kaersutite, and liquid are shown in Fig. 6. The compositions of all phases were recast into normative constituents and the Ab, Or, and An molar abundances renormalized. The normative An/Or ratio of the kaersutite remains essentially invariant across the path **A–B–C*–D**. Because the normative Ab content of kaersutite is strongly dependent

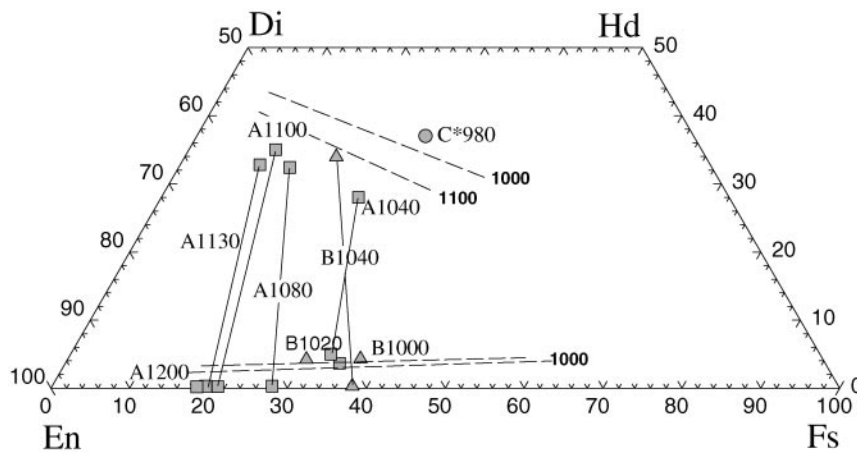


Fig. 5. Compositions of olivine (along En–Fs sideline) and pyroxene (within quadrilateral) along the path A–B–C*–D at 9.3 kbar plotted as QUIIF projections. Tie-lines indicate coexisting phases. Dashed lines represent isotherms of the augite–orthopyroxene solvus, calculated using the method of Andersen *et al.* (1993). Temperatures are indicated as in Fig. 3.

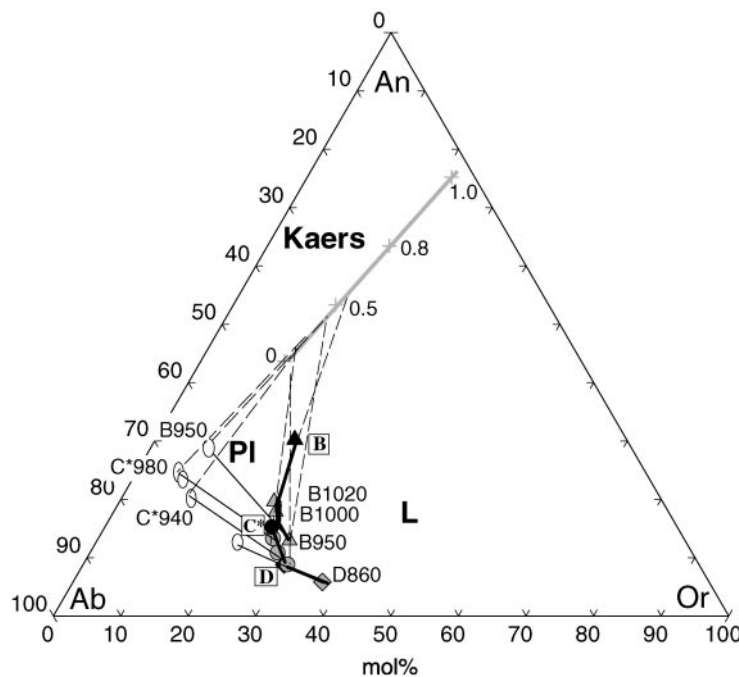


Fig. 6. Experimental plagioclase (Pl, open ovals) and renormalized normative feldspar compositions of liquid (L, gray symbols) and kaersutite (Kaers) at 9.3 kbar. Black symbols are those of Fig. 3; the boxed labels **B**, **C***, **D** refer to bulk compositions in Table 1. Temperature symbols are as in Fig. 3. The kaersutite compositional variation as a function of FeO/FeO_T is shown by the bold gray curve. The kaersutite composition in bulk composition **C*** at 980°C is shown with varying FeO/FeO_T by the + symbol and indicated numerically along the curve.

upon $\text{FeO}/(\text{FeO} + \text{Fe}_2\text{O}_3)$, the kaersutite compositions plot increasingly towards the Ab apex with increasing relative Fe^{3+} , forming the straight line shown in Fig. 6. Kaersutite–liquid tie-lines were approximated as the tangents to the liquid line of descent in the plagioclase-free regime. Interestingly, they suggest kaersutite with rather high Fe^{3+} /total Fe ratios [consistent with the results of King *et al.* (1999)], and an increase in this ratio with

falling temperature. Once feldspar crystallizes, these tie-lines indicate only the presence of kaersutite.

Liquids evolving from **B** move initially away from kaersutite and hence become rapidly An-poor before undergoing the Or enrichment that accompanies the crystallization of plagioclase. Liquids emanating from **C*** mirror the latter part of this trend. The offset of the liquid paths reflects the change in bulk composition from

Table 4: Representative residual liquid compositions and phase assemblages of 'dry' experiments at 9.3 kbar

| Starting material: | A* | A* | A* | A* | A* |
|-----------------------------------|--------------------------------|------------------------------|-----------------------|----------------------------|--------------------------------|
| Bulk water content (wt %): | 'Dry' | <0.05 | 0.05 ¹ | 0.38 ¹ | 0.64 ¹ |
| Equilibration temperature (°C): | 1250 | 1170 | 1160 | 1140 | 1140 |
| SiO ₂ | 48.51 | 45.55 | 48.04 | 47.28 | 48.19 |
| TiO ₂ | 2.74 | 4.92 | 3.33 | 5.02 | 3.17 |
| Al ₂ O ₃ | 15.02 | 14.76 | 16.02 | 14.51 | 16.68 |
| FeO _T | 10.84 | 13.32 | 10.95 | 13.13 | 10.01 |
| MnO | 0.13 | 0.20 | 0.12 | 0.15 | 0.11 |
| MgO | 8.45 | 4.07 | 5.06 | 4.63 | 4.97 |
| CaO | 9.26 | 6.48 | 7.73 | 7.71 | 8.02 |
| Na ₂ O | 2.89 | 3.56 | 3.44 | 3.45 | 3.54 |
| K ₂ O | 1.48 | 2.92 | 1.84 | 2.50 | 1.77 |
| P ₂ O ₅ | 49.00 | 1.17 | 0.63 | 0.99 | 0.68 |
| Total | 99.81 | 96.94 | 97.24 | 99.37 | 97.14 |
| Molar Mg no. | 62 | 39 | 51 | 43 | 51 |
| Phases | L | Ol + Cpx + Pl + Il + L | Ol + Cpx + Pl + L | Ol + Cpx + Pl + tr. Il + L | Ol + Cpx + L |
| Water in residual glass (wt %) | | | 0.08 | 0.6 | 0.8 |
| Crystallinity (wt %); s.s.r. <0.4 | 0 | 56 (21% Pl; 28% Cpx; tr. Il) | 34 (7% Pl; 18% Cpx) | 36 (26% Pl; 19% Cpx) | 20 (14% Cpx) |
| Starting material: | A* | B* | B* | B* | B* |
| Bulk water content (wt %): | 0.37 ¹ | 'Dry' | 0.42 ¹ | 0.04 ¹ | 0.41 ¹ |
| Equilibration temperature (°C): | 1100 | 1250 | 1140 | 1120 | 1100 |
| SiO ₂ | 48.92 | 48.53 | 48.07 | 45.82 | 48.90 |
| TiO ₂ | 3.35 | 2.87 | 3.05 | 4.51 | 2.94 |
| Al ₂ O ₃ | 16.20 | 15.31 | 15.55 | 13.87 | 15.07 |
| FeO _T | 10.94 | 11.76 | 11.23 | 12.68 | 11.99 |
| MnO | 0.15 | 0.15 | 0.12 | 0.19 | 0.16 |
| MgO | 3.62 | 5.93 | 4.58 | 4.04 | 2.79 |
| CaO | 6.36 | 7.73 | 7.56 | 7.53 | 5.58 |
| Na ₂ O | 3.99 | 3.64 | 3.92 | 3.77 | 4.56 |
| K ₂ O | 3.15 | 2.19 | 2.39 | 2.94 | 4.31 |
| P ₂ O ₅ | 1.28 | 1.65 | 1.80 | 2.66 | 1.86 |
| Total | 97.96 | 99.76 | 98.27 | 98.01 | 98.16 |
| Molar Mg | 43 | 51 | 46 | 40 | 33 |
| Phases | Ol + Cpx + Pl + Il + Ap + L | L | Ol + Cpx + Pl + L | Ol + Cpx + Pl + L | Ol + Cpx + Pl + Ap + Il + L |
| Water in residual glass (wt %) | 0.8 | | 0.46 | 0.07 | 1.16 |
| Crystallinity (wt %); s.s.r. <0.4 | 54 (21% Pl; 17% Cpx; 18% Ol) | 0 | 8 (3.7% Ol; 2.9% Cpx) | 38 (23% Pl; 11% Ol) | 65 (34% Pl; 12% Cpx; 15% Ol) |

¹Estimated initial water content computed from measured water content of residual glass and calculated crystallinity.

B to **C***. Liquids of **D** composition crystallize sodic plagioclase early; this produces strong **K** enrichment and the stabilization of biotite. A two-feldspar assemblage is not stable for any composition along this path. This is

consistent with the ternary feldspar models (as applied through SOLVCALC; Wen & Nekvasil, 1994) of Nekvasil & Burnham (1983, 1984), Fuhrman & Lindsley (1988), Lindsley & Nekvasil (1989) and Elkins & Grove (1990).

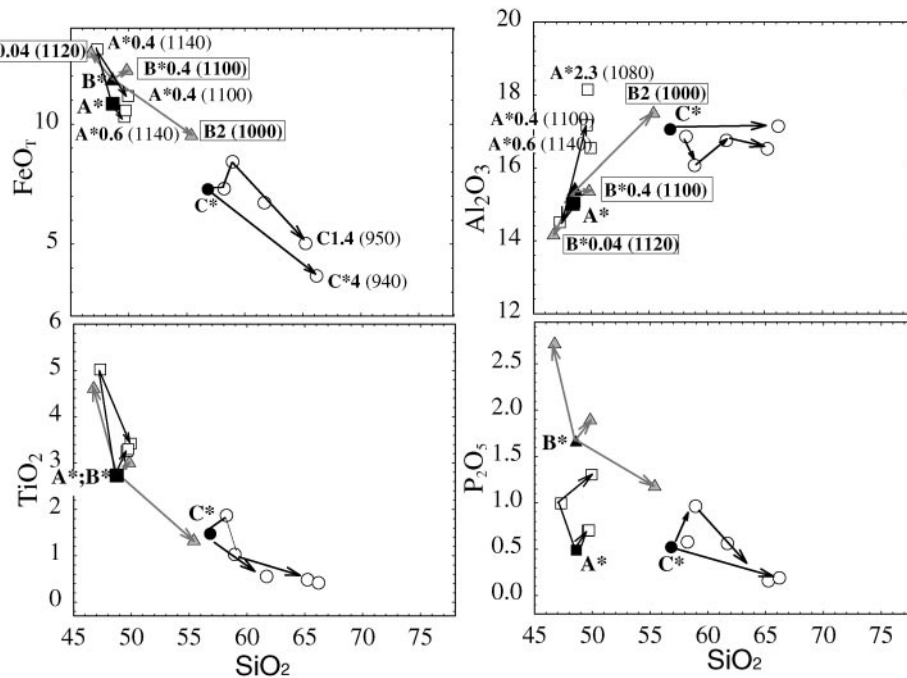


Fig. 7. Harker variation diagrams showing the variations in liquid line of descent for compositions **A***, **B***, and **C*** with variable bulk water contents. Bulk compositions are shown by black symbols. Other symbols represent experimental residual liquids. Symbol shapes are keyed to bulk compositions. Labels give first bulk composition, then bulk water content (in wt %), and, in parenthesis, temperature in °C. Arrows indicate the down-temperature direction.

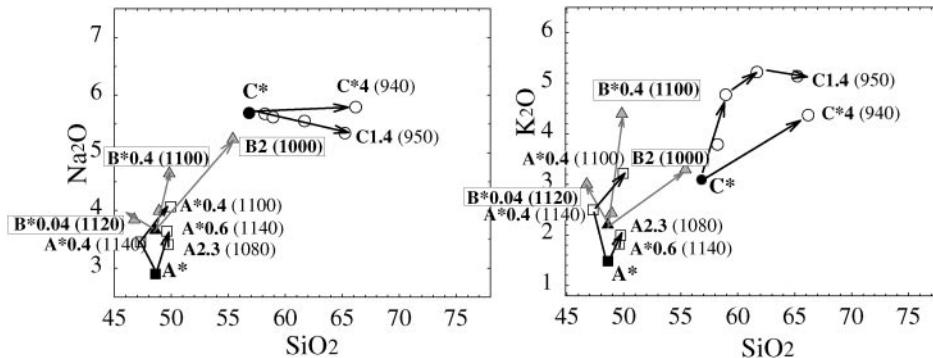


Fig. 8. Harker variation diagrams showing the variations in alkali contents for compositions **A***, **B***, and **C*** with variable bulk water contents. Symbols and labels as in Fig. 7.

None of these models indicate that the feldspar solidus intersects the ternary feldspar solvus at any of the temperatures of the experiments.

'Low' water contents

The liquid line of descent is affected strongly by bulk water content. For bulk composition **A*** (where the asterisk indicates a change in bulk water content from that of the natural rock **A** of Table 1) with dissolved water contents of 0.4 wt % or less, plagioclase becomes a major crystallizing phase accompanied by clinopyroxene and olivine (Table 4) and the liquid is marked by early silica and alumina depletion, and Fe, Ti and P enrichment before

the liquids begin to undergo silica enrichment (Fig. 7). In this way, basalts produced along this 'dry' path can have rather low Mg numbers and alumina content, and high Ti and P contents relative to the starting hawaiite (Fig. 7), without much change in silica. Trachyandesite composition **B*** mirrors this behavior. With very low bulk water contents, it produces the same type of early silica depletion trend (Fig. 7) as produced for **A***. The extent of silica and alumina depletion, and Fe, Ti and P enrichment is moderated by increased water content of the starting material. The change in liquid line of descent with bulk water content is demonstrated well for **B*** in Figs 7 and 8 (with 0.04, 0.6 and 2 wt % bulk water contents).

Table 5: Representative mineral compositions for the 'dry' experiments of Table 4

| Starting material: | A* | A* | A* | A* | A* | A* | A* |
|---------------------------------|--|---|--|--|---|--|--|
| Bulk water content (wt %): | <0.05 | <0.05 | <0.05 | 0.05 ¹ | 0.05 ¹ | 0.05 ¹ | 0.38 ¹ |
| Equilibration temperature (°C): | 1170 | 1170 | 1170 | 1160 | 1160 | 1160 | 1140 |
| Phase: | clinopyroxene | olivine | plagioclase | clinopyroxene | olivine | plagioclase | clinopyroxene |
| SiO ₂ | 48.04 | 35.73 | 56.02 | 49.55 | 40.76 | 53.58 | 49.81 |
| TiO ₂ | 2.22 | 0.15 | 0.18 | 1.88 | 1.10 | 0.06 | 2.43 |
| Al ₂ O ₃ | 5.83 | 0.06 | 25.99 | 6.66 | 5.51 | 28.65 | 5.90 |
| FeO _T | 11.04 | 31.95 | 0.37 | 8.32 | 20.75 | 0.24 | 10.50 |
| MnO | 0.22 | 0.29 | 0.01 | 0.16 | 0.22 | 0.00 | 0.24 |
| MgO | 13.83 | 29.27 | 0.08 | 15.66 | 27.00 | 0.09 | 14.68 |
| CaO | 15.27 | 0.34 | 8.73 | 16.72 | 2.57 | 11.45 | 16.00 |
| Na ₂ O | 0.67 | 0.03 | 5.25 | 0.71 | 1.11 | 4.38 | 0.75 |
| K ₂ O | 0.01 | 0.01 | 1.63 | 0.01 | 0.60 | 0.59 | 0.22 |
| P ₂ O ₅ | 0.03 | 0.10 | 0.04 | 0.05 | 0.36 | 0.04 | 0.13 |
| Total | 97.13 | 97.93 | 98.29 | 99.71 | 99.99 | 99.07 | 100.70 |
| Phase comp. (mol %) | En ₅₀ Wo ₂₉ Fs ₂₁ | Fo ₆₁ Fa ₃₈ (0.5) | An ₄₃ Ab ₄₇ Or ₁₀ | En ₅₅ Wo ₂₈ Fs ₁₇ | Fo ₇₃ Fa ₂₇ (0.1) | An ₅₇ Ab ₄₀ Or ₃ | En ₅₀ Wo ₃₄ Fs ₁₆ |
| Starting material: | A* | A* | A* | A* | A* | B* | B* |
| Bulk water content (wt %): | 0.38 ¹ | 0.38 ¹ | 0.37 ¹ | 0.37 ¹ | 0.37 ¹ | 0.42 ¹ | 0.42 ¹ |
| Equilibration temperature (°C): | 1140 | 1140 | 1100 | 1100 | 1100 | 1140 | 1140 |
| Phase: | olivine | plagioclase | clinopyroxene | olivine | plagioclase | clinopyroxene | olivine |
| SiO ₂ | 49.07 | 55.61 | 49.01 | 36.68 | 55.68 | 50.06 | 37.34 |
| TiO ₂ | 2.39 | 0.18 | 2.28 | 0.11 | 0.19 | 1.74 | 0.09 |
| Al ₂ O ₃ | 5.81 | 27.84 | 6.25 | 0.02 | 27.29 | 5.64 | 0.00 |
| FeO _T | 10.34 | 0.50 | 10.13 | 31.62 | 0.41 | 9.39 | 27.99 |
| MnO | 0.24 | 0.00 | 0.26 | 0.33 | 0.01 | 0.09 | 0.31 |
| MgO | 14.46 | 0.09 | 14.23 | 31.25 | 0.12 | 15.57 | 34.00 |
| CaO | 15.76 | 10.05 | 17.25 | 0.25 | 9.84 | 16.26 | 0.26 |
| Na ₂ O | 0.74 | 5.27 | 0.53 | 0.05 | 5.50 | 0.55 | 0.01 |
| K ₂ O | 0.22 | 1.08 | 0.03 | 0.00 | 1.01 | 0.07 | 0.00 |
| P ₂ O ₅ | 0.13 | 0.05 | 0.02 | 0.14 | 0.06 | 0.11 | 0.20 |
| Total | 100.00 | 100.70 | 99.97 | 100.47 | 100.12 | 99.47 | 100.19 |
| Phase comp. (mol %) | Fo ₆₇ Fa ₃₃ (0.55) | An ₄₉ Ab ₄₅ Or ₆ | En ₄₉ Wo ₃₂ Fs ₁₉ | Fo ₆₄ Fa ₃₆ (0.44) | An ₄₇ Ab ₄₈ Or ₅ | En ₅₄ Wo ₂₈ Fs ₁₈ | Fo ₆₈ Fa ₃₂ (0.37) |

The experiments provide constraints on the water contents needed to generate the silica-saturated alkalic path from mildly alkalic hawaiite. A minimum bulk water content between 0.4 and 0.6 wt % (i.e. ~0.5 wt %) is required to replicate the natural trend of bulk compositions from **A*** (Figs 7 and 8). An important effect of water content on the liquid lines of descent that start out below this minimum value is a marked change in Na₂O/(Na₂O + K₂O). During the early stages of crystallization, under conditions of either high or low bulk water contents, K acts almost as an element incompatible with the crystalline assemblages, as the plagioclase crystallizing at

low bulk water contents is still relatively low in Or component and the kaersutite crystallizing at higher bulk water contents is sodic. However, at low bulk water contents, the presence of sodic plagioclase (Table 5) in the crystallizing assemblage inhibits major increases in Na₂O content of the residual liquids. This, when coupled with the small changes in silica with crystallization as the melt switches from a silica-depletion to a silica-enrichment trend, results in strongly potassic (but still *hy*-normative) compositions, even though the starting materials all lie on the typical sodic alkalic trend. This can be clearly seen also for liquids derived from **C** (1.4 wt % water; Fig. 8, Table 6).

Table 5: continued

| Starting material: | B* | B* | B* | B* | B* | B* | B* |
|---------------------------------|---|--|---|---|--|---|--|
| Bulk water content (wt %): | 0.42 ¹ | 0.04 ¹ | 0.04 ¹ | 0.04 ¹ | 0.41 ¹ | 0.41 ¹ | 0.41 ¹ |
| Equilibration temperature (°C): | 1140 | 1120 | 1120 | 1120 | 1100 | 1100 | 1100 |
| Phase: | plagioclase | clinopyroxene | olivine | plagioclase | clinopyroxene | olivine | plagioclase |
| SiO ₂ | 55.98 | 49.31 | 36.88 | 56.66 | 47.01 | 35.09 | 56.94 |
| TiO ₂ | 0.07 | 2.27 | 0.46 | 0.15 | 3.26 | 0.12 | 0.24 |
| Al ₂ O ₃ | 27.61 | 5.69 | 1.88 | 26.72 | 5.77 | 0.42 | 25.51 |
| FeO _T | 0.15 | 10.46 | 29.04 | 0.35 | 10.67 | 36.60 | 0.69 |
| MnO | 0.00 | 0.20 | 0.29 | 0.00 | 0.24 | 0.45 | 0.00 |
| MgO | 0.08 | 13.28 | 26.59 | 0.10 | 11.57 | 24.71 | 0.10 |
| CaO | 9.74 | 17.40 | 0.93 | 9.08 | 19.26 | 0.41 | 8.05 |
| Na ₂ O | 5.23 | 0.66 | 0.32 | 5.55 | 0.79 | 0.26 | 5.53 |
| K ₂ O | 0.97 | 0.11 | 0.36 | 1.31 | 0.01 | 0.09 | 1.96 |
| P ₂ O ₅ | 0.01 | 0.15 | 0.40 | 0.01 | 0.23 | 0.32 | 0.14 |
| Total | 99.84 | 99.53 | 97.15 | 99.91 | 98.80 | 98.46 | 99.15 |
| Phase comp. (mol %) | An ₄₈ Ab ₄₆ Or ₆ | En ₄₆ Wo ₃₃ Fs ₂₁ | Fo ₆₁ Fa ₃₅ (0.5) | An ₄₃ Ab ₄₉ Or ₈ | En ₄₄ Wo ₃₅ Fs ₂₁ | An ₂₆ Ab ₆₈ Or ₆ | An ₃₉ Ab ₅₀ Or ₁₁ |

¹Estimated initial water content computed from measured water content of residual glass and calculated crystallinity. Temperatures in bold indicate change from previous listed temperature.

The plagioclase compositions of Table 5 do not lie along a specific crystallization path because of the different bulk starting water contents of the experiments for the same anhydrous bulk composition. However, where the degree of crystallinity is similar, the higher temperatures of the experiments with low water contents clearly show the predicted more ternary nature of the plagioclase compositions. None of the ‘dried’ experimental products yielded a two-feldspar assemblage. This is consistent with the ternary feldspar solution models of Ghiorso (1984), Nekvasil & Burnham (1987), Fuhrman & Lindsley (1988), Lindsley & Nekvasil (1989) and Elkins & Grove (1990). Only the model of Green & Usdansky (1986) incorrectly predicts the presence of two feldspars.

The compositions of experimental feldspars and the renormalized normative feldspar compositions of the residual liquids from **A*** (Table 5) are shown in Fig. 9. For consistency with the liquid projection scheme, renormalized normative feldspar constituents of the coexisting pyroxene (Table 5) are also plotted. These constituents reflect the Ca-Tschermaks component (CaTs) in the pyroxene, which is not considered in the standard norm calculation procedure and can result in artificially elevated normative An content of the coexisting liquid. For the high-temperature assemblages here, mass balance can be met only if these pyroxene constituents are taken into account. The importance of this consideration to mass balance can be readily seen in Fig. 9. Without

inclusion of the pyroxenes, the plagioclase/liquid tie-lines would not intersect the bulk composition.

Phase relations at intermediate and low pressure

The differences between the fractionating assemblage at 9.3 kbar and the natural assemblages observed in the rocks suggest the possibility of a change in crystalline assemblage after decompression. To evaluate the possibility of such change and provide limits on the pressure range over which the bulk liquid compositions of the suite can be generated, experiments were conducted at 4.3 and 3.8 kbar and ~1 atm.

Table 7 and Figure 10 show the major element compositions of liquids produced by crystallization of **B** at 4.3 kbar NVA. Abundant early crystallization of plagioclase and olivine in **B** (2 wt % water) instead of pyroxene results in a major difference in liquid evolution path. This difference is particularly evident in the Na₂O and Al₂O₃ vs SiO₂ diagrams of Fig. 10. The early plagioclase precipitation inhibits the early buildup of Na₂O and alumina characteristic of the main alkalic trend, whereas olivine and kaersutite precipitation drives the melt quickly towards silica enrichment. The almost incompatible increase in K₂O content results in strong changes in the Na₂O/(Na₂O + K₂O) ratio and the formation of strongly potassic (yet still silica-saturated) compositions

Table 6: Representative residual liquid and mineral compositions C at 9.3 kbar

| Starting material: | C | C | C | C | C | C |
|--|--|---|--|---|--|--|
| Bulk water content (wt %): | 1.4 (NVA) | 1.4 | 1.4 | 1.4 | 1.4 | 1.4 |
| Equilibration temperature (°C): | 1250 | 1060 | 1040 | 1020 | 970 | 950 |
| SiO ₂ | 56.42 | 56.53 | 56.47 | 57.02 | 57.55 | 63.46 |
| TiO ₂ | 1.46 | 1.81 | 1.71 | 0.99 | 0.51 | 0.47 |
| Al ₂ O ₃ | 16.93 | 16.37 | 15.74 | 15.54 | 15.63 | 16.06 |
| FeO _T | 7.22 | 7.09 | 8.17 | 8.15 | 6.27 | 4.89 |
| MnO | 0.09 | 0.11 | 0.12 | 0.12 | 0.04 | 0.07 |
| MgO | 2.71 | 1.67 | 1.34 | 1.02 | 0.60 | 0.39 |
| CaO | 5.06 | 3.77 | 2.97 | 2.91 | 2.02 | 1.51 |
| Na ₂ O | 5.65 | 5.51 | 5.68 | 5.43 | 5.18 | 2.91 (5.2) |
| K ₂ O | 3.07 | 3.68 | 4.07 | 4.61 | 4.87 | 5.00 |
| P ₂ O ₅ | 0.52 | 0.56 | 0.70 | 0.93 | 0.52 | 0.16 |
| Total | 99.13 | 97.10 | 96.25 | 96.72 | 93.20 | 94.92 |
| Molar Mg no. | 44 | 33 | 26 | 21 | 17 | 14 |
| Phases | L | Pl + Cpx + L | Pl + Cpx + Il + L | Pl + Cpx + Il + L | Pl + Cpx + Il + Bt + L | Pl + Cpx + Il + Bt + Kaers + L |
| Crystallinity (vol. %); s.s.r. <0.417 | | 9 (8% Cpx) | 43 (29% Pl; 13% Cpx) | 64 (45% Pl; 18% Cpx) | 83 (57% Pl; 16% Cpx; 9% Bt) | 87 (58% Pl; 17% Cpx; 11% Bt) |
| Starting material: | C | C | C | C | C | C |
| Bulk water content (wt %): | 1.4 | 1.4 | 1.4 | 1.4 | 1.4 | 1.4 |
| Equilibration temperature (°C): | 1060 | 1060 | 1040 | 1040 | 1020 | 1020 |
| Phase: | clinopyroxene | plagioclase | clinopyroxene | plagioclase | clinopyroxene | plagioclase |
| SiO ₂ | 48.65 | 60.42 | 49.97 | 60.59 | 49.79 | 61.35 |
| TiO ₂ | 1.85 | 0.14 | 1.44 | 0.24 | 1.67 | 0.16 |
| Al ₂ O ₃ | 5.12 | 24.55 | 4.93 | 23.62 | 4.78 | 22.92 |
| FeO _T | 12.21 | 0.29 | 16.09 | 0.73 | 20.34 | 0.42 |
| MnO | 0.31 | 0.03 | 0.38 | 0.00 | 0.52 | 0.00 |
| MgO | 12.40 | 0.01 | 11.39 | 0.11 | 9.22 | 0.03 |
| CaO | 17.41 | 6.29 | 14.02 | 5.38 | 10.35 | 4.88 |
| Na ₂ O | 0.70 | 7.19 | 0.89 | 7.23 | 0.85 | 7.16 |
| K ₂ O | 0.00 | 1.25 | 0.15 | 1.65 | 0.56 | 2.06 |
| P ₂ O ₅ | 0.08 | 0.05 | 0.07 | 0.08 | 0.21 | 0.08 |
| Total | 98.74 | 100.21 | 99.34 | 99.55 | 98.29 | 99.04 |
| Phase comp. (mol %) | En ₄₃ Wo ₃₄ Fs ₂₃ | An ₃₀ Ab ₆₃ Or ₇ | En ₄₁ Wo ₂₇ Fs ₃₂ | An ₂₇ Ab ₆₄ Or ₉ | En ₃₇ Wo ₂₉ Fs ₃₄ | An ₂₃ Ab ₆₅ Or ₁₂ |

reminiscent of the intermediate rocks of provinces such as the Snake River Plain (e.g. Stout *et al.*, 1994) and the Massif Anorthosite Complexes. At lower water contents (**B**^{*}, 0.06 wt % water), the absence of kaersutite diminishes the increase in silica content per degree of crystallization, but the greater abundance of olivine relative to clinopyroxene impedes the strong Fe enrichment of the magma that occurs at higher pressure (Table 7 and Fig. 10).

Decompression of trachytic liquid (**C**^{*}, 3.5 wt % water) and crystallization at 4.3 kbar results in an early

plagioclase- rather than kaersutite-dominated assemblage and residual liquids that differ markedly from any found in the typical sodic silica-saturated alkalic suites (Tables 7 and 8, and Fig. 10). The lack of overlap of the liquid lines of descent of trachyandesite (**B**, 2 wt % water) (Fig. 10) and trachyte (alkali syenite, **C**^{*}) at 4.3 kbar shows clearly that they cannot be related by fractionation at this pressure.

Experiments at 0 kbar on **A** show early olivine domination that drives the liquid towards high silica contents

Table 6: continued

| Starting material: | C | C | C | C | C | C |
|---------------------------------|--|--|---------|--|--|---------|
| Bulk water content (wt %): | 1.4 | 1.4 | 1.4 | 1.4 | 1.4 | 1.4 |
| Equilibration temperature (°C): | 970 | 970 | 970 | 950 | 950 | 950 |
| Phase: | clinopyroxene | plagioclase | biotite | clinopyroxene | plagioclase | biotite |
| SiO ₂ | 50.22 | 63.17 | 38.78 | 49.24 | 62.09 | 33.32 |
| TiO ₂ | 0.58 | 0.14 | 7.75 | 0.83 | 0.07 | 8.43 |
| Al ₂ O ₃ | 2.06 | 22.56 | 13.49 | 4.02 | 22.89 | 13.44 |
| FeO _T | 23.17 | 0.39 | 19.38 | 20.88 | 0.30 | 24.85 |
| MnO | 0.57 | 0.01 | 0.02 | 0.56 | 0.00 | 0.19 |
| MgO | 11.61 | 0.03 | 6.95 | 8.60 | 0.05 | 6.98 |
| CaO | 11.39 | 4.55 | 0.44 | 13.08 | 4.66 | 0.11 |
| Na ₂ O | 0.35 | 7.18 | 1.06 | 0.85 | 7.64 | 0.90 |
| K ₂ O | 0.02 | 2.64 | 7.60 | 0.69 | 1.98 | 8.07 |
| P ₂ O ₅ | 0.02 | 0.07 | 0.21 | 0.10 | 0.09 | 0.04 |
| Total | 97.00 | 100.74 | 95.67 | 98.84 | 99.77 | 96.32 |
| Phase comp. (mol %) | En ₃₆ Wo ₂₃ Fs ₄₁ | An ₂₂ Ab ₆₂ Or ₁₅ | | En ₃₁ Wo ₂₆ Fs ₄₃ | An ₂₁ Ab ₆₅ Or ₁₁ | |

Temperatures in bold indicate change from previous listed temperature.

(Fig. 11). This yields a liquid line of descent that deviates strongly from the silica-saturated alkalic path and is most similar to fractionation products of ocean island olivine tholeiites.

No experimental assemblage produced two feldspars at 4.3 kbar for bulk compositions **A**, **B** and **C*** (3.5 wt % H₂O). Plagioclase crystallization begins at an earlier stage than at higher pressure. The early plagioclase crystallization at intermediate pressures results in the stability of plagioclase that is more calcic than that which crystallized at 9.3 kbar from trachyandesite **B** (Fig. 12). Early plagioclase domination drives the liquid to higher normative Or contents at 4.3 kbar relative to 9.3 kbar (Fig. 12) and strongly decreases the Na/K ratio of the liquids.

Olivine/pyroxene equilibria also change as a function of pressure. Consistent with the observations of other workers (e.g. Thompson, 1974; Longhi & Bertka, 1996), the clinopyroxene becomes increasingly calcic with decreasing pressure. At 0 kbar, Fe–Ti spinel commonly coexists with clinopyroxene and olivine. This assemblage allowed the QUIIF method of Andersen *et al.* (1993) to be used to calculate the f_{O_2} (relative to a standard state of pure O₂ gas at 298 K, 1 atm). These calculations were also performed when spinel and ilmenite coexisted with or without ferromagnesian minerals. Table 9 shows the calculated results relative to the FMQ buffer (see also Table 10). The calculated f_{O_2} varies between 1.5 and 2 log units above FMQ at each temperature of the 0 kbar experiments, with a general decreasing trend with falling

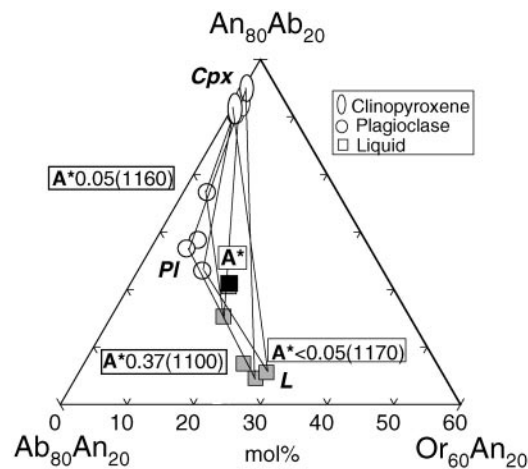


Fig. 9. Plagioclase (○), renormalized normative feldspar compositions of coexisting liquid (gray squares), and normative feldspar constituents of coexisting pyroxene (open ovals) for composition **A*** (■) at 9.3 kbar and the conditions of Table 4. Labels indicate the bulk water content and equilibration temperature (after melting at 1250°C) of the experiment. Tie-lines connect coexisting phases. Because of the variation in bulk water contents, these data do not indicate a crystallization path.

temperature. As a note of caution, however, these 0 kbar silica-tube experiments differ significantly from the higher-pressure piston-cylinder experiments. Thus, the 0 kbar f_{O_2} results need not bear any relationship to the higher-pressure experimental conditions.

Table 7: Representative residual liquid compositions and phase assemblages at 4.3 kbar and 3.8 kbar

| | | | | |
|-------------------------------------|--------------------------------------|---|---|--|
| Pressure (kbar): | 4.3 | 4.3 | 4.3 | 4.3 |
| Starting material: | B | B | B | B |
| Bulk water content (wt %): | 2 (NVA) | 2 (NVA) | 0.21 ¹ | 0.35 ¹ |
| Equilibration temperature (°C): | 1050 | 1000 | 1120 | 1100 |
| SiO ₂ | 51.26 | 57.77 | 48.21 | 48.82 |
| TiO ₂ | 2.95 | 0.90 | 2.93 | 3.59 |
| Al ₂ O ₃ | 15.11 | 16.78 | 15.50 | 14.13 |
| FeO _T | 10.14 | 5.26 | 11.35 | 11.40 |
| MnO | 0.17 | 0.08 | 0.12 | 0.15 |
| MgO | 2.87 | 0.96 | 5.32 | 3.58 |
| CaO | 6.65 | 2.83 | 7.76 | 7.72 |
| Na ₂ O | 3.60 | 4.10 | 3.69 | 3.54 |
| K ₂ O | 3.20 | 5.68 | 2.25 | 3.02 |
| P ₂ O ₅ | 1.28 | 0.33 | 1.59 | 1.91 |
| Total | 97.24 | 94.68 | 98.71 | 97.85 |
| Molar Mg no. | 43 | 25 | 49 | 41 |
| Phases | Ol + Pl + Il + Ap + L | Ol + Pl + Il + Ap + Kaers + Bt + L | Ol + L | Ol + Pl + Il + Ap + L |
| Water in residual glass (wt %) | | | 0.21 | 0.52 |
| Crystallinity (vol. %); s.s.r. <0.4 | 28 (13% Pl; 13% Ol; 0.5% Il) | 66 (17% Pl; 10% Ol; 1% Il; 35% Kaers; Bt) | 2 | 33 (20% Pl; 11% Ol; 0.8% Il) |
| Pressure (kbar): | 4.3 | 4.3 | 4.3 | 3.8 |
| Starting material: | B* | C* | C* | E |
| Bulk water content (wt %): | 0.06 ¹ | 3.5 | 3.5 | 4 (NVA) |
| Equilibration temperature (°C): | 1080 | 940 | 920 | 940 |
| SiO ₂ | 50.53 | 61.86 | 64.95 | 68.01 |
| TiO ₂ | 3.48 | 0.45 | 0.43 | 0.56 |
| Al ₂ O ₃ | 13.76 | 16.60 | 15.83 | 14.64 |
| FeO _T | 11.67 | 3.99 | 4.10 | 2.99 |
| MnO | 0.16 | 0.01 | 0.08 | 0.06 |
| MgO | 2.84 | 0.31 | 0.29 | 0.29 |
| CaO | 6.95 | 1.56 | 1.12 | 1.42 |
| Na ₂ O | 4.00 | 4.95 | 3.64 | 3.13(3.2) |
| K ₂ O | 3.79 | 5.47 | 5.11 | 6.58 |
| P ₂ O ₅ | 1.79 | 0.13 | 0.10 | 0.13 |
| Total | 98.98 | 95.32 | 95.63 | 97.80 |
| Molar Mg no. | 35 | 14 | 13 | 17 |
| Phases | Ol + Pl + Il + Ap + Cpx + L | Cpx + Pl + Mgt + Ap + Kaers + Bt + L | Cpx + Pl + Mgt + Ap + Kaers + Bt + L | Ol + Cpx + Pl + Il + Ap + Bt + L |
| Water in residual glass (wt %) | 0.15 | | | |
| Crystallinity (vol. %); s.s.r. <0.4 | 58 (37% Pl; 16% Ol; 2% Il; 1% Ap) | 71 (43% Pl; 8% Cpx; 8% Bt; 11% Kaers; 1% Ap) | 99 (64% Pl; 11% Cpx; 13% Bt; 10% Kaers; 1% Ap) | 75 (51% Pl; 2% Cpx; 2% Il; 12% Ol; 6.5% Bt) |

¹Estimated initial water content computed from measured water content of residual glass and calculated crystallinity.

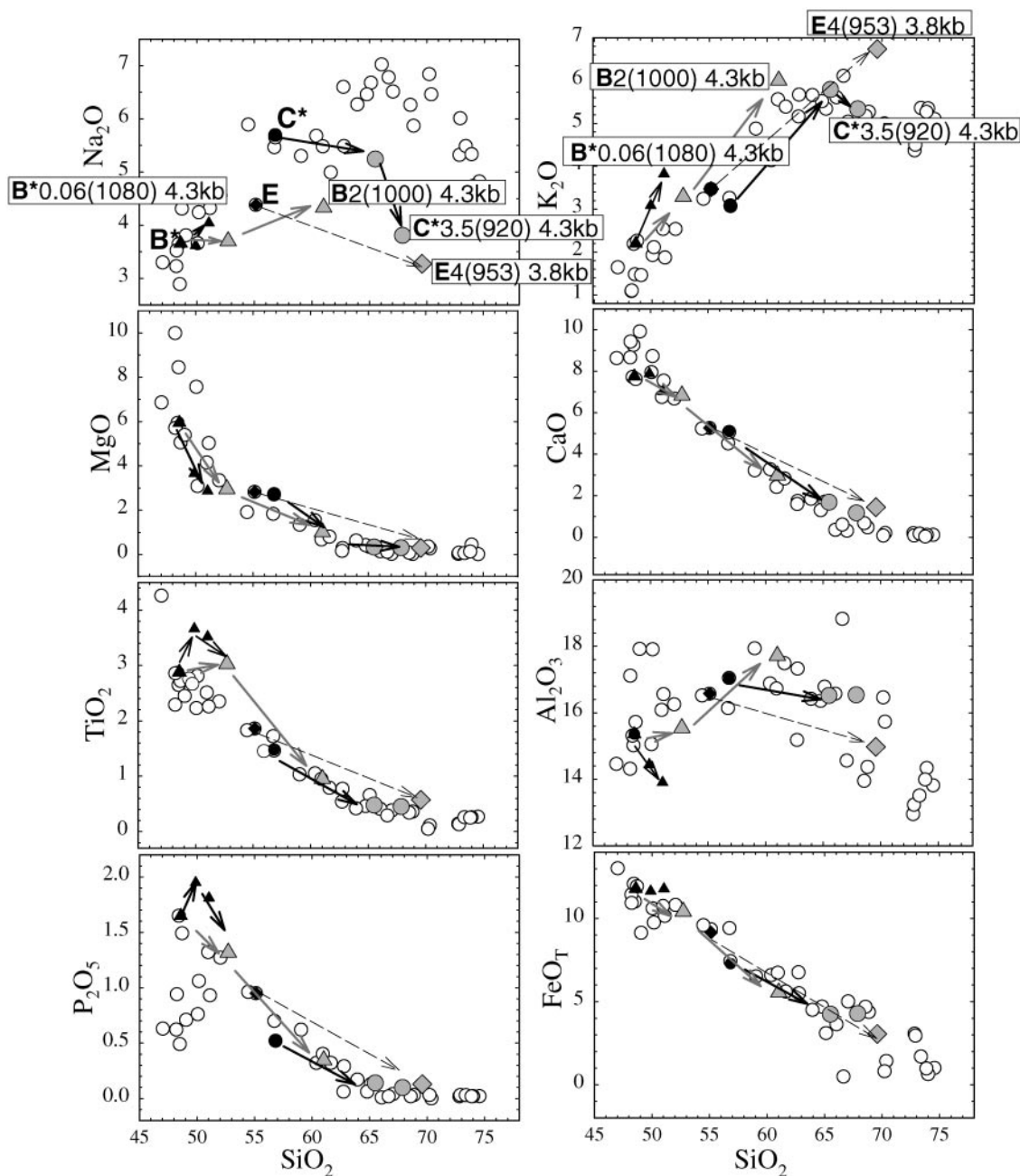


Fig. 10. Harker variation diagrams of residual liquid compositions (gray symbols) for bulk compositions **B*** and **C*** at 4.3 kbar for variable water contents, and **E** at 3.8 kbar. Arrows indicate the down-temperature direction. Labels indicate the starting composition, bulk water content, equilibration temperature (after melting at 1250°C) in parenthesis, and pressure of each experiment. \circ , bulk compositions for the Nandewar suite (Abbott, 1969; Stolz, 1985).

DISCUSSION

Agreement between experimental residual liquids along the fractionation path and bulk-rock compositions of natural silica-saturated alkalic suites provide compelling evidence that the compositional variations of bulk lava

compositions, from olivine basalt to rhyolite, in such suites of the ocean island and continental 'anorogenic' regimes could arise primarily from fractional crystallization of a mildly alkalic hawaiite at depths of ~ 30 km. Mineralogical evidence that the basaltic magmas of such

Table 8: Representative mineral compositions from experiments of Table 7

| | | | | | | |
|---------------------------------|---|---|---|---|--|--|
| Pressure (kbar): | 4.3 | 4.3 | 4.3 | 4.3 | 4.3 | 4.3 |
| Starting material: | B | B | B | B | B | B |
| Bulk water content (wt %): | 2 (NVA) | 2 (NVA) | 2 (NVA) | 2 (NVA) | 2 (NVA) | 2 (NVA) |
| Equilibration temperature (°C): | 1050 | 1050 | 1000 | 1000 | 1000 | 1000 |
| Phase: | olivine | plagioclase | olivine | plagioclase | pigeonite | kaersutite |
| SiO ₂ | 35.50 | 54.24 | 33.83 | 0.11 | 49.86 | 41.68 |
| TiO ₂ | 0.11 | 0.10 | 0.13 | 28.35 | 1.72 | 5.04 |
| Al ₂ O ₃ | 0.00 | 29.27 | 0.00 | 0.00 | 7.10 | 10.92 |
| FeO _T | 32.14 | 0.29 | 40.79 | 0.30 | 13.15 | 15.79 |
| MnO | 0.41 | 0.00 | 0.62 | 0.00 | 0.28 | 0.21 |
| MgO | 30.62 | 0.07 | 23.01 | 0.02 | 12.41 | 10.99 |
| CaO | 0.27 | 10.42 | 0.33 | 8.87 | 13.04 | 9.75 |
| Na ₂ O | 0.05 | 4.97 | 0.00 | 5.29 | 0.90 | 1.80 |
| K ₂ O | 0.01 | 0.64 | 0.01 | 0.98 | 0.98 | 0.92 |
| P ₂ O ₅ | 0.63 | 0.00 | 0.30 | 0.00 | 0.13 | 0.4 |
| Total | 99.74 | 100.00 | 99.02 | 100.59 | 99.57 | 97.57 |
| Phase comp. (mol %) | Fo ₆₁ Fa ₃₈ (0.5) | An ₅₂ Ab ₄₄ Or ₄ | Fo ₅₀ Fa ₅₀ (0.5) | An ₄₃ Ab ₅₂ Or ₅ | En ₄₈ Fs ₂₉ Wo ₂₃ | |
| Pressure (kbar): | 4.3 | 4.3 | 4.3 | 4.3 | 4.3 | 4.3 |
| Starting material: | B* | B* | B* | B* | B* | B* |
| Bulk water content (wt %): | 0.21 ¹ | 0.35 ¹ | 0.35 ¹ | 0.06 ¹ | 0.06 ¹ | 0.06 ¹ |
| Equilibration temperature (°C): | 1120 | 1100 | 1100 | 1080 | 1080 | 1080 |
| Phase: | olivine | olivine | plagioclase | olivine | plagioclase | clinopyroxene |
| SiO ₂ | 36.33 | 35.93 | 54.67 | 35.41 | 55.88 | 47.72 |
| TiO ₂ | 0.11 | 0.18 | 0.15 | 0.17 | 0.24 | 3.63 |
| Al ₂ O ₃ | 0.00 | 0.03 | 27.15 | 0.01 | 26.08 | 4.51 |
| FeO _T | 24.59 | 30.93 | 0.25 | 36.46 | 0.46 | 9.88 |
| MnO | 0.28 | 0.37 | 0.00 | 0.51 | 0.00 | 0.20 |
| MgO | 35.61 | 30.00 | 0.09 | 25.97 | 0.08 | 12.03 |
| CaO | 0.32 | 0.49 | 9.68 | 0.50 | 9.58 | 20.43 |
| Na ₂ O | 0.01 | 0.02 | 5.39 | 0.00 | 5.27 | 0.61 |
| K ₂ O | 0.03 | 0.03 | 0.87 | 0.06 | 1.31 | 0.02 |
| P ₂ O ₅ | 0.36 | 0.08 | 0.02 | 0.18 | 0.05 | 0.07 |
| Total | 97.63 | 98.07 | 98.27 | 99.08 | 98.91 | 99.03 |
| Phase comp. (mol %) | Fo ₇₂ Fa ₂₈ (0.4) | Fo ₆₃ Fa ₃₇ (0.7) | An ₄₇ Ab ₄₇ Or ₆ | Fo ₅₆ Fa ₄₄ (0.8) | An ₄₄ Ab ₄₈ Or ₈ | En ₄₀ Wo ₄₂ Fs ₁₈ |

suites experienced some degree of crystallization at this depth is preserved in occasional pyroxene megacrysts. Figure 13 delineates the effect of pressure on the cation abundances of Ti vs total Al in experimental clinopyroxenes. When compared with the experimental pyroxenes, natural megacrystic, phenocrystic and groundmass clinopyroxenes of the Nandewar mafic rocks, for example, show a systematic variation with pressure, with the megacrysts lying at pressures consistent with 30–40 km depth, and the phenocrysts and microlites at decreasing pressure (Fig. 13). Such evidence of a polybaric

history preserved in pyroxene is not unique to the Nandewar suite and is seen in other silica-saturated alkalic suites (e.g. pyroxenes from the Warrumbungle volcano, Australia, shown in Fig. 13; Ghorbani & Middlemost, 2000).

The major differences in liquid lines of descent at intermediate and low pressures relative to the high-pressure path and the evident preservation of the high-pressure path indicate that fractionation did not occur at pressures below that of the main fractionation event. Thus, the polybaric nature of the natural

Table 8: continued

| | | | | | | |
|---------------------------------|--|---|--|-----------------------------------|--|--|
| Pressure (kbar): | 4-3 | 4-3 | 4-3 | 4-3 | 4-3 | 4-3 |
| Starting material: | C* | C* | C* | C* | C* | C* |
| Bulk water content (wt%): | 3-5 | 3-5 | 3-5 | 3-5 | 3-5 | 3-5 |
| Equilibration temperature (°C): | 940 | 940 | 940 | 940 | 920 | 920 |
| Phase: | clinopyroxene | plagioclase | kaersutite | biotite | clinopyroxene | plagioclase |
| SiO ₂ | 50-56 | 62-10 | 39-74 | 34-39 | 48-48 | 62-99 |
| TiO ₂ | 0-53 | 0-09 | 5-83 | 8-87 | 1-26 | 0-00 |
| Al ₂ O ₃ | 1-41 | 23-83 | 11-24 | 13-83 | 4-85 | 20-82 |
| FeOT | 29-23 | 0-31 | 19-09 | 18-16 | 16-77 | 1-01 |
| MnO | 0-78 | 0-00 | 0-30 | 0-07 | 0-44 | 0-00 |
| MgO | 11-27 | 0-03 | 7-23 | 8-32 | 8-34 | 0-07 |
| CaO | 4-97 | 5-82 | 10-29 | 0-04 | 17-97 | 2-93 |
| Na ₂ O | 0-26 | 7-39 | 2-57 | 1-06 | 0-62 | 7-41 |
| K ₂ O | 0-24 | 1-29 | 0-96 | 7-19 | 0-06 | 3-12 |
| P ₂ O ₅ | 0-03 | 0-10 | 0-22 | 0-03 | 0-30 | 0-33 |
| Total | 99-26 | 100-95 | 97-46 | 91-97 | 99-09 | 98-70 |
| Phase comp. (mol %) | En ₃₃ Wo ₁₈ Fs ₄₉ | An ₂₈ Ab ₆₅ Or ₇ | | | En ₃₁ Wo ₃₅ Fs ₃₄ | An ₁₃ Ab ₆₈ Or ₁₉ |
| Pressure (kbar): | 4-3 | 4-3 | 3-8 | 3-8 | 3-8 | 3-8 |
| Starting material: | C* | C* | E | E | E | E |
| Bulk water content (wt%): | 3-5 | 3-5 | 4 (NVA) | 4 (NVA) | 4 (NVA) | 4 (NVA) |
| Equilibration temperature (°C): | 920 | 920 | 940 | 940 | 940 | 940 |
| Phase: | kaersutite | biotite | clinopyroxene | olivine | plagioclase | Ba-rich biotite |
| SiO ₂ | 38-85 | 37-25 | 49-42 | 32-16 | 60-63 | 27-35 |
| TiO ₂ | 4-56 | 7-42 | 1-73 | 0-19 | 0-08 | 9-13 |
| Al ₂ O ₃ | 10-60 | 14-06 | 3-84 | 0-05 | 23-49 | 12-38 |
| FeOT | 22-07 | 20-73 | 15-07 | 48-84 | 0-25 | 23-42 |
| MnO | 0-35 | 0-15 | 0-47 | 0-97 | 0-02 | 0-22 |
| MgO | 6-67 | 6-21 | 10-19 | 15-09 | 0-02 | 4-72 |
| CaO | 10-53 | 0-21 | 17-97 | 0-34 | 6-53 | 0-06 |
| Na ₂ O | 2-68 | 1-24 | 0-39 | 0-04 | 6-45 | 0-42 |
| K ₂ O | 0-83 | 7-20 | 0-09 | 0-04 | 2-08 | 3-29 |
| P ₂ O ₅ | 0-14 | 0-07 | 0-09 | 0-63 | 0-15 | 0-04 |
| Total | 97-38 | 94-56 | 99-24 | 98-35 | 99-68 | 81-02 |
| Phase comp. (mol%) | | | En ₃₅ Wo ₃₆ Fs ₂₉ | Fo ₃₅ Fa ₆₄ | An ₂₉ Ab ₅₉ Or ₁₂ | |

¹Estimated initial water content computed from measured water content of residual glass and calculated crystallinity. Temperatures in bold indicate change from previous listed temperature.

mineral assemblage provides evidence only for several additional stages of ponding and crystallization, but not for additional fractionation stages. This observation readily circumvents the problems encountered by workers such as Stolz (1985) when trying to computationally fractionate hawaiite to produce trachyandesite using the mineral assemblages observed in the lavas.

The observation that liquids become more alkalic during fractionation of a pyroxene-dominated assemblage suggests that the primary criterion for producing the alkalic liquids in these suites is not so much inherited alkalic characteristics of the parent liquid, but rather attainment of conditions that suppress early crystallization of plagioclase and induce early crystallization of an olivine-poor, pyroxene-dominated assemblage. Taking this

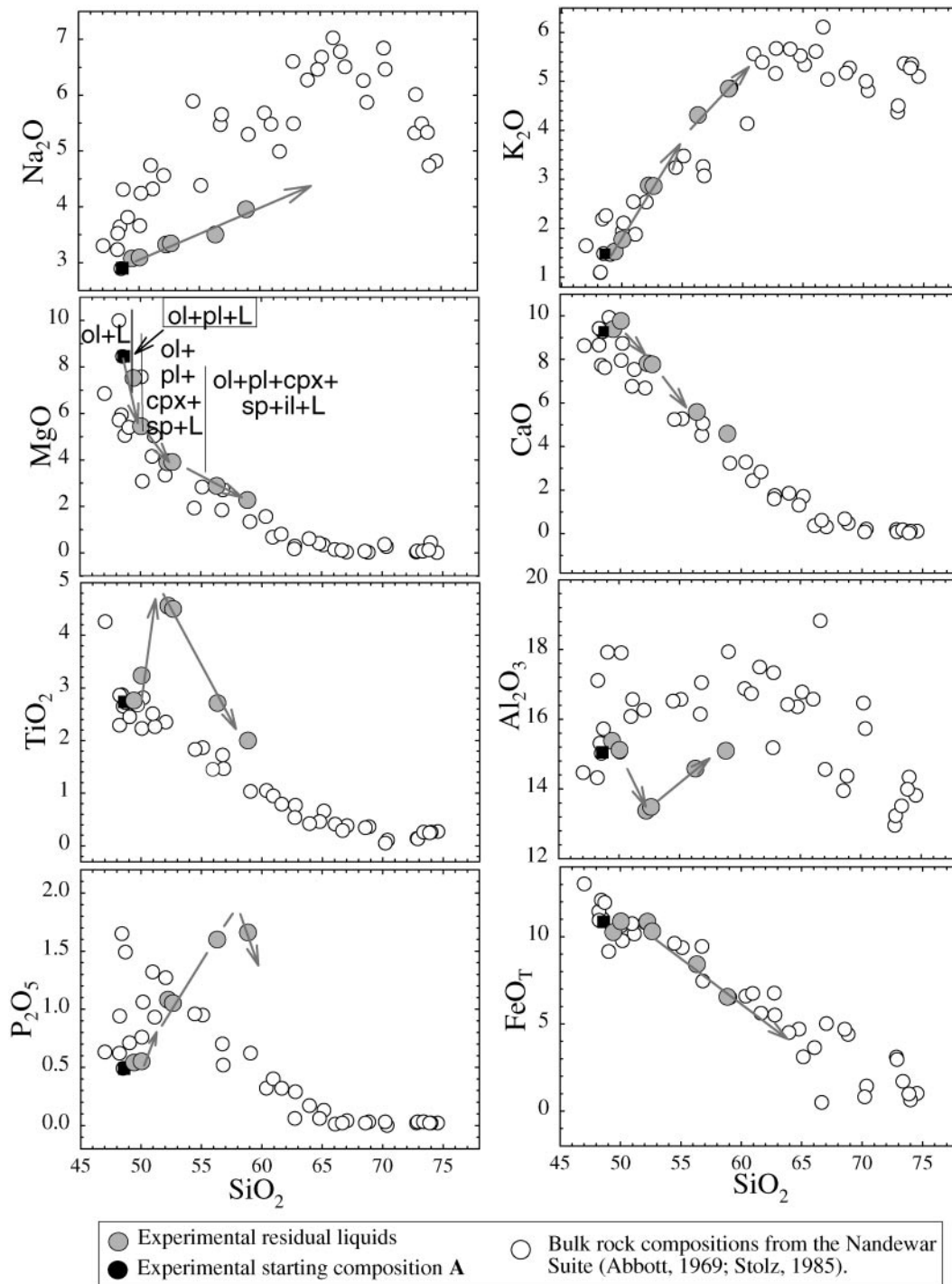


Fig. 11. Harker variation diagrams of residual liquid compositions (gray circles) for bulk composition A* (<0.04 wt % H₂O; ■) at 0 kbar. Phase assemblages along the experimental path: ol, olivine; pl, plagioclase; cpx, clinopyroxene; sp, spinel; il, ilmenite; L, liquid. Arrows indicate the down-temperature direction. Temperatures are given in Table 9.

further, if such conditions could be found for the olivine tholeiite commonly associated with alkalic suites, then perhaps the tholeiite could give rise to the mildly alkalic hawaiite and the remainder of the suite. Pressure and,

perhaps even more importantly, water content are critical variables in the suppression of feldspar crystallization. At 9.3 kbar, it was observed that plagioclase crystallization becomes sufficiently suppressed to permit hawaiite to

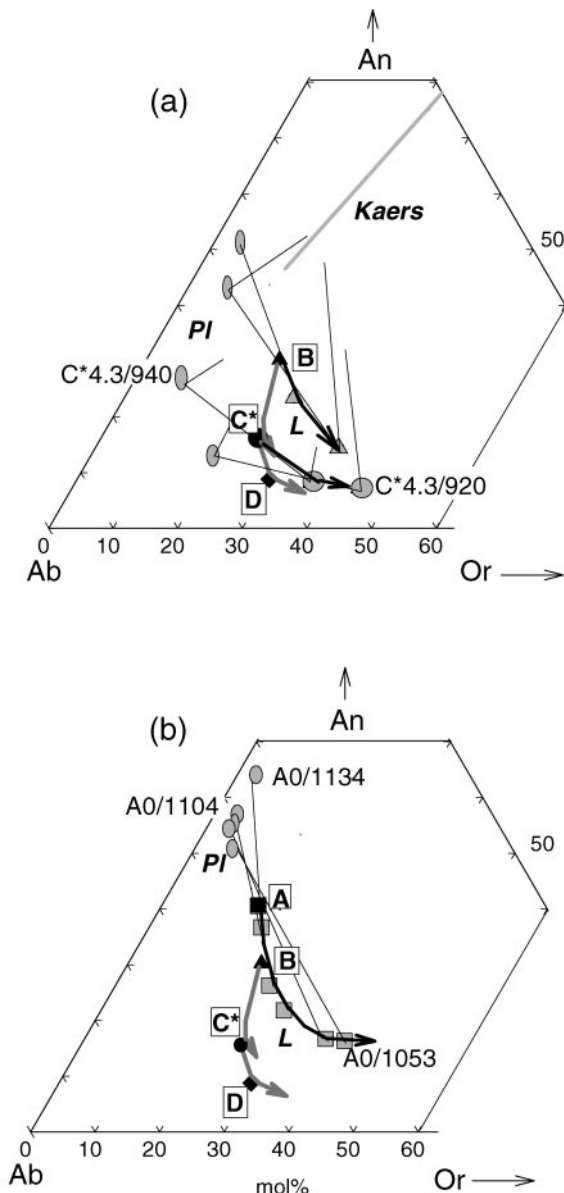


Fig. 12. Renormalized normative feldspar compositions for the phases plagioclase (PI, ovals), liquid (L) and kaersutite (Kaers) obtained experimentally at 4.3 kbar (a) and plagioclase and liquid at 0 kbar (open symbols) (b). Black symbols show bulk compositions **A**, **B**, and **C*** (3.5 wt % H₂O) and **D**. Gray symbols indicate experimental residual liquids. Labels (e.g. C*4.3/940) give bulk composition, pressure, and temperature) of an experimental datum. Projected kaersutite compositional variation with FeO/FeO_T at 4.3 kbar is shown by the bold gray line. The liquid lines of descent from **B** and **C*** at 4.3 kbar are indicated by black curves in (a) and from **A** at 0 kbar by the black curve in (b). Gray curves in (a) and (b) show the 9.3 NVA liquid lines of descent from **B** and **C*** for comparison. Tie-lines indicate coexisting phases. Partial three-phase triangles in (a) indicate kaersutite-bearing assemblages.

become more strongly alkalic if the bulk water content is greater than ~0.5 wt %. Although this is also the case at 4.3 kbar, residual liquids become strongly potassic (i.e. high K₂O/Na₂O ratios) at lower pressure, thereby losing

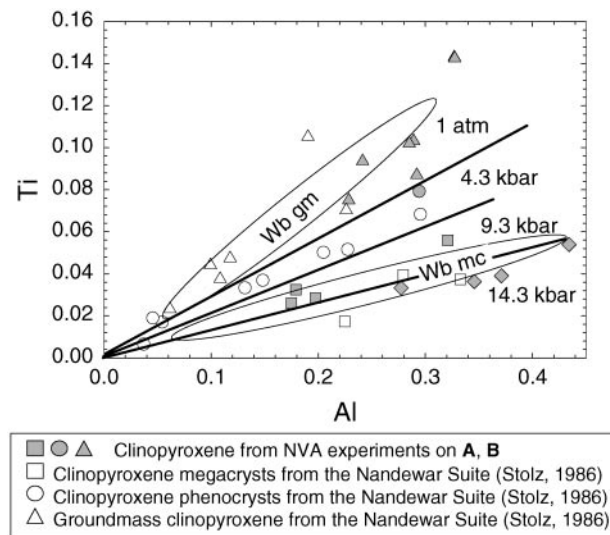


Fig. 13. Ti vs total Al (atomic proportions for 6 O) of natural clinopyroxenes of the Nandewar basalts (Stolz, 1986) (open symbols) and synthetic pyroxenes (gray symbols). Elliptical outlines indicate field of natural Warrumbungle groundmass (Wb gm) and megacrystic (Wb mc) pyroxenes (Ghorbani & Middlemost, 2000). Pressures are indicated for experimental pyroxenes. Pressure boundaries are approximate. Data for 14.3 kbar are from J. Filiberto (personal communication, 2002). (As a note of caution, although the pressure effects on pyroxene composition indicated in this figure are probably applicable to pyroxenes in rocks similar to the hawaiite used here, this diagram should be used with caution when applied to grossly different liquid compositions and crystallization conditions because it is based on the presence of only a single pyroxene rather than two-pyroxene equilibria.)

the sodic characteristics common to these suites. At 9.3 kbar, water contents below this minimum produce markedly different liquid lines of descent that show the silica depletion and Fe, Ti and P enrichment characteristic of hotspot suites such as Craters of the Moon (e.g. Stout *et al.*, 1994).

Fractionation has been shown to be a viable mechanism for producing many of the compositionally diverse members of this suite-type. However, this does not prove that this process took place exclusively or even in part in natural systems and other possible mechanisms must be considered. It is generally recognized that assimilation can produce major changes in liquid evolution (e.g. Ghiorsio & Kelemen, 1987). A felsic assimilant in basalt, for example, can produce liquids that are more alkali- and silica-rich than the initial basalt; however, it is difficult to envision the type of assimilant that would produce the initial strong increase in alkalis that is characteristic of the transition from hawaiite to trachyandesite without affecting silica content. A felsic assimilant may be more effective in changing a tristanite to a trachytic composition. Evidence for this should show up in the isotopic and trace element characteristics of the affected magmas if they were significantly different in the melt and assimilant (Reiners *et al.*, 1995). No evidence for this

Table 9: Representative residual liquid compositions and phase assemblages at 0 kbar

| Starting material: | A | A | A | A | A | A |
|--|--------|------------------|--------------------------------|---------------------------------|--|--|
| Equilibration temperature (°C): | 1181 | 1134 | 1104 | 1089 | 1065 | 1053 |
| SiO ₂ | 48.99 | 48.76 | 50.00 | 51.68 | 54.69 | 58.51 |
| TiO ₂ | 2.74 | 3.15 | 4.36 | 4.51 | 2.63 | 1.99 |
| Al ₂ O ₃ | 15.24 | 14.74 | 12.57 | 13.22 | 14.16 | 15.00 |
| FeO _T | 10.25 | 10.58 | 11.34 | 10.53 | 8.17 | 6.50 |
| MnO | 0.14 | 0.12 | 0.13 | 0.19 | 0.11 | 0.10 |
| MgO | 7.46 | 5.30 | 4.92 | 3.85 | 2.80 | 2.25 |
| CaO | 9.39 | 9.50 | 9.41 | 7.74 | 5.42 | 4.56 |
| Na ₂ O | 3.07 | 3.01 | 3.02 | 3.29 | 3.39 | 3.39 |
| K ₂ O | 1.52 | 1.73 | 2.19 | 2.84 | 4.18 | 4.82 |
| P ₂ O ₅ | 0.54 | 0.53 | 0.79 | 1.07 | 1.55 | 1.65 |
| Total | 99.34 | 97.42 | 98.72 | 98.91 | 97.12 | 98.77 |
| Molar Mg no. | 61 | 51 | 47 | 44 | 43 | 42 |
| Phases | Ol + L | Ol + Plag + L | Ol + Plag + Cpx + Sp + L | Ol + Plag + Cpx + Sp + L | Ol + Plag + Cpx + Sp + Il + L | Ol + Plag + Cpx + Sp + Il + L |
| Crystallinity (vol. %); s.s.r. <0.4 | 2% Ol | 17 (9% Ol) | 52 (13% Ol; 29% Pl; 3% Cpx) | 64 (15% Ol; 36% Pl; 10% Cpx) | 73 (15% Ol; 36% Pl; 17% Cpx; 4% Sp) | 75 (15% Ol; 35% Pl; 20% Cpx; 3% Il) |
| DFMQ | | | 1.96 | 1.53 | 1.68 | 1.46 |

DFMQ, log units below the fayalite–magnetite–quartz buffer.

has been reported for these suites, in spite of the diverse geological settings in which hotspots and continental rifts are found.

The experimental results also constrain the possible role of partial melting in generating the intermediate units of these suites. Equilibrium crystallization (as well as the incremental fractionation experiments) of hawaiiite (A) has produced trachytic compositions; thus, theoretically speaking, it should be possible to produce trachytic compositions by partial melting of hawaiiite. It was observed, however, that the higher the magmatic water content, the greater the amount of trachyte produced during crystallization. Thus, fluid availability and composition in the hawaiitic source will severely constrain the efficacy of this process.

Whether or not rhyolites can be produced by equilibrium crystallization or melting was not resolved in the experiments presented, but it has been verified that mafic rhyolites can be produced by fractionation. The likelihood of some direct relationship of alkali-rich rhyolites to the associated mafic and intermediate units is supported by similar isotopic signatures (although the most evolved trachytes and rhyolites commonly deviate somewhat in Sr isotope systematics, e.g. Kar *et al.*, 1998) and by various field relationships. Fast-cooled dike swarms of continental plutonic alkalic provinces (e.g. the Gardar province) show direct continuity from basalt to trachyte

and comendite (Upton & Emeeus, 1987). Silica-saturated alkalic volcanic sequences commonly show intimate associations of felsic rocks with trachytes [e.g. felsic bottom units grading upward into more voluminous trachytic ashflow tuffs (Gibson, 1970; Villari, 1975); thin layers of peralkaline trachyte and grading upward into massive trachyte (Stolz, 1985)] that imply roofward silica enrichment within a magma chamber. These relationships are coupled to enrichment in Na, Fe, Mn, F, Cl, Rb, Cs, Pb, Th, U, Nb, Ta, Zr, Hf, REE, Y, Zn, F and Cl, and depletion in Mg, Al, K, Ca, Ti, P, Sc and Ba in the rhyolitic units (e.g. Menengai, Kenya; Macdonald, 1987). These enriched elements are all strongly complexed in aqueous fluids with Cl and F (e.g. Webster, 1997) and their enrichment is consistent with volatile mobility. Perhaps, as suggested by Bailey & Macdonald (1975), the alkali rhyolites arise by coupled fractionation and roofward alkali and silica enrichment by a rising halogen-rich vapor that cools near the roof of the magma chamber. The fractionation paths evaluated here cannot be used to assess this possibility as they do not take into account the effects of dissolved halogens. Halogen abundance and effects are likely to be particularly important in late-stage liquids and may play a major role in the evolution of the most felsic members of the silica-saturated alkalic suites; further work is needed to assess their effects.

Table 10: Representative mineral compositions at 0 kbar from the experiments of Table 9

| | | | | | | | |
|---------------------------------|---|---|--|---|--|--|--|
| Starting material: | A | A | A | A | A | A | A |
| Equilibration temperature (°C): | 1181 | 1134 | 1134 | 1104 | 1104 | 1104 | 1104 |
| Phase: | olivine | olivine | plagioclase | olivine | plagioclase | clinopyroxene | spinel |
| SiO ₂ | 40.29 | 38.61 | 51.82 | 38.90 | 54.36 | 45.92 | 0.08 |
| TiO ₂ | 0.07 | 0.12 | 0.18 | 0.04 | 0.23 | 2.91 | 14.48 |
| Al ₂ O ₃ | 0.07 | 0.15 | 29.48 | 0.01 | 28.27 | 4.95 | 3.70 |
| FeO _T | 14.32 | 17.43 | 0.95 | 21.22 | 1.33 | 8.99 | 66.95 |
| MnO | 0.19 | 0.22 | 0.02 | 0.36 | 0.01 | 0.15 | 0.38 |
| MgO | 45.29 | 41.24 | 0.23 | 39.41 | 0.17 | 13.06 | 5.81 |
| CaO | 0.22 | 0.39 | 13.50 | 0.35 | 12.38 | 20.73 | 0.29 |
| Na ₂ O | 0.03 | 0.12 | 3.82 | 0.02 | 4.33 | 0.40 | 0.00 |
| K ₂ O | 0.01 | 0.08 | 0.35 | 0.01 | 0.53 | 0.00 | 0.08 |
| P ₂ O ₅ | 0.49 | 0.05 | 0.00 | 0.08 | 0.04 | 0.08 | 0.09 |
| Total | 100.98 | 98.40 | 100.34 | 100.39 | 101.64 | 97.20 | 91.70 |
| Phase comp. (mol %) | For ₈₅ Fa ₁₅ (0.29) | For ₈₀ Fa ₁₉ (0.55) | An ₆₄ Ab ₃₄ Or ₂ | For ₇₆ Fa ₂₃ (0.48) | An ₅₇ Ab ₄₀ Or ₃ | En ₅₀ Wo ₄₀ Fs ₁₀ | Usp ₄₄ Mt ₅₆ |
| Starting material: | A | A | A | A | A | A | A |
| Equilibration temperature (°C): | 1089 | 1089 | 1089 | 1089 | 1065 | 1065 | 1065 |
| Phase: | olivine | plagioclase | clinopyroxene | spinel | olivine | plagioclase | clinopyroxene |
| SiO ₂ | 38.71 | 53.58 | 51.15 | 0.19 | 37.24 | 54.40 | 44.04 |
| TiO ₂ | 0.39 | 0.30 | 1.77 | 17.00 | 0.08 | 0.24 | 4.35 |
| Al ₂ O ₃ | 1.45 | 27.63 | 1.98 | 3.42 | 0.05 | 26.97 | 5.19 |
| FeO _T | 22.27 | 1.38 | 8.53 | 66.04 | 22.95 | 1.10 | 10.15 |
| MnO | 0.35 | 0.00 | 0.23 | 0.32 | 0.33 | 0.05 | 0.19 |
| MgO | 34.53 | 0.30 | 16.05 | 5.75 | 37.27 | 0.30 | 11.35 |
| CaO | 1.03 | 12.03 | 19.52 | 0.30 | 0.32 | 11.02 | 20.75 |
| Na ₂ O | 0.63 | 4.42 | 0.26 | 0.05 | 0.01 | 4.63 | 0.50 |
| K ₂ O | 0.25 | 0.62 | 0.01 | 0.04 | 0.01 | 0.69 | 0.02 |
| P ₂ O ₅ | 0.20 | 0.08 | 0.04 | 0.03 | 0.09 | 0.03 | 0.28 |
| Total | 99.81 | 100.32 | 99.55 | 93.13 | 98.39 | 99.91 | 96.84 |
| Phase comp. (mol %) | For ₇₃ Fa ₂₆ (0.57) | An ₅₅ Ab ₄₁ Or ₄ | En ₄₈ Wo ₄₀ Fs ₁₃ | Usp ₅₁ Mt ₄₉ | For ₇₄ Fa ₂₆ (0.46) | An ₅₄ Ab ₄₂ Or ₄ | En ₄₂ Wo ₄₃ Fs ₁₅ |
| Starting material: | A | A | A | A | A | A | A |
| Equilibration temperature (°C): | 1065 | 1065 | 1053 | 1053 | 1053 | 1053 | 1053 |
| Phase: | spinel | ilmenite | olivine | plagioclase | clinopyroxene | spinel | ilmenite |
| SiO ₂ | 0.25 | 0.20 | 36.73 | 53.96 | 46.28 | 2.23 | 2.35 |
| TiO ₂ | 16.48 | 44.41 | 0.07 | 0.40 | 3.19 | 14.50 | 40.26 |
| Al ₂ O ₃ | 3.11 | 0.50 | 0.09 | 25.78 | 4.24 | 3.25 | 1.03 |
| FeO _T | 64.73 | 41.63 | 27.00 | 1.98 | 10.10 | 68.84 | 45.73 |
| MnO | 0.35 | 0.34 | 0.38 | 0.05 | 0.16 | 0.32 | 0.29 |
| MgO | 4.90 | 5.87 | 33.53 | 0.32 | 12.21 | 5.45 | 4.94 |
| CaO | 0.39 | 0.47 | 0.35 | 10.61 | 20.73 | 0.34 | 0.47 |
| Na ₂ O | 0.04 | 0.01 | 0.01 | 4.66 | 0.48 | 0.13 | 0.10 |
| K ₂ O | 0.04 | 0.03 | 0.02 | 0.96 | 0.03 | 0.11 | 0.23 |
| P ₂ O ₅ | 0.02 | 0.00 | 0.05 | 0.13 | 0.24 | 0.06 | 0.09 |
| Total | 90.30 | 93.45 | 98.23 | 98.83 | 97.65 | 95.23 | 95.49 |
| Phase comp. (mol %) | Usp ₅₁ Mt ₄₉ | Ilm ₈₃ Hem ₁₇ | For ₆₉ Fa ₃₁ (0.51) | An ₅₃ Ab ₄₂ Or ₆ | En ₄₁ Wo ₄₁ Fs ₁₈ | Usp ₄₃ Mt ₅₇ | Il ₇₅ Hem ₂₅ |

Temperatures in bold indicate change from previous listed temperature.

ACKNOWLEDGEMENTS

The authors would like to thank J. Longhi, T. Naumann and B. J. Upton for thoughtful reviews, and the University of Armidale and The Australian National University for samples from the Nandewar volcano. This work was supported by NSF grant EAR0000926, which is gratefully acknowledged.

REFERENCES

- Abbott, M. J. (1969). Petrology of the Nandewar volcano. N.S.W. Australia. *Contributions to Mineralogy and Petrology* **20**, 115–134.
- Andersen, D. J., Lindsley, D. H. & Davidson, P. M. (1993). QUILF; a Pascal program to assess equilibria among Fe–Mg–Mn–Ti oxides, pyroxenes, olivine, and quartz. *Computers and Geosciences* **19**(9), 1333–1350.
- Bailey, D. K. (1964). Crustal warping, a possible tectonic control of alkaline magmatism. *Journal of Geophysical Research* **69**(6), 1103–1111.
- Bailey, D. K. (1974). Origin of alkaline magmas as a result of anatexis. In: Sorensen, H. (ed.) *Alkaline Rocks*. New York: John Wiley, pp. 427–442.
- Bailey, D. K. & Macdonald, R. (1975). Fluorine and chlorine in peralkaline liquids and the need for magma generation in an open system. *Mineralogical Magazine* **40**, 405–414.
- Barberi, F., Ferrara, G., Santacroce, R., Treuil, M. & Varet, J. (1975). A transitional basalt–pantellerite sequence of fractional crystallization, the Boina Centre (Afar Rift, Ethiopia). *Journal of Petrology* **16**(1), 22–56.
- Bowen, N. L. (1937). Recent high-temperature research on silicates and their significance in igneous geology. *American Journal of Science* **33**, 1–21.
- Bryan, W. B. (1967). Geology and petrology of Clarion Island, Mexico. *Geological Society of America Bulletin* **78**, 1461–1476.
- Carmichael, I. S. E. & Ghiorso, M. S. (1990). The effect of oxygen fugacity on the redox state of natural liquids and their crystallizing phases. *Reviews in Mineralogy* **24**, 191–212.
- Carr, M. E. (2000). *IgPet for Windows*. Somerset, NJ: Terra Softa Inc.
- Dixon, J. E., Stolper, E. M. & Holloway, J. R. (1995). An experimental study of water and carbon dioxide solubilities in mid-ocean ridge basaltic liquids. Part I: Calibration and solubility models. *Journal of Petrology* **36**, 1607–1631.
- Downes, H. (1987). Tertiary and Quaternary volcanism in the Massif Central, France. In: Fitton, J. G. & Upton, B. G. J. (eds) *The Alkaline Igneous Rocks*. Boston, MA: Blackwell Scientific, pp. 517–530.
- Elkins, L. & Grove, T. L. (1990). Ternary feldspar experiments and thermodynamic models. *American Mineralogist* **75**(5–6), 544–559.
- Ewart, A. (1981). The mineralogy and chemistry of the anorogenic Tertiary silicic volcanism of SE Queensland and NE New South Wales, Australia. *Journal of Geophysical Research* **86**, 10242–10256.
- Fuhrman, M. L. & Lindsley, D. H. (1988). Ternary-feldspar modeling and thermometry. *American Mineralogist* **73**(3–4), 201–215.
- Ghiorso, M. S. (1984). Activity/composition relations in the ternary feldspars. *Contributions to Mineralogy and Petrology* **87**(3), 282–296.
- Ghiorso, M. S. & Kelemen, P. B. (1987). Evaluating reaction stoichiometry in magmatic systems evolving under generalized thermodynamic constraints: examples comparing isothermal and isenthalpic assimilation. In: Mysen, B. O. (ed.) *Magmatic Processes: Physicochemical Principles*. Geochemical Society, Special Publication **1**, 319–336.
- Ghorbani, M. R. & Middlemost, E. A. K. (2000). Geochemistry of pyroxene inclusions from the Warrumbungle Volcano, New South Wales, Australia. *American Mineralogist* **85**, 1349–1367.
- Gibson, I. L. (1970). A pantelleritic welded ash-flow tuff from the Ethiopian Rift Valley. *Contributions to Mineralogy and Petrology* **28**, 89–111.
- Green, N. L. & Usdansky, S. I. (1986). Ternary feldspar mixing relations and thermobarometry. *American Mineralogist* **71**(1–2), 1100–1108.
- Haase, K. M., Stoffers, P. & Garbe-Schönberg, C. P. (1997). The petrogenetic evolution of lavas from Easter Island and neighbouring seamounts, near-ridge hotspot volcanoes in the SE Pacific. *Journal of Petrology* **38**, 785–813.
- Harris, C. (1983). The petrology of lavas and associated plutonic inclusions of Ascension Island. *Journal of Petrology* **24**, 424–470.
- Irvine, T. N. & Baragar, W. R. A. (1971). A guide to the chemical classification of the common volcanic rocks. *Canadian Journal of Earth Sciences* **8**, 523–548.
- Johnson, R. W., O'Reilly, S. Y., Lister, G. S., Etheridge, M. A., Knutson, S., Sun, S. S., Ewart, A., Green, D. H., McDonough, W. F. & Wellman, P. (1989). *Intraplate Volcanism in Eastern Australia and New Zealand*. Cambridge: Cambridge University Press, 408 pp.
- Kar, A., Weaver, B., Davidson, J. & Colucci, M. (1998). Origin of differentiated volcanic and plutonic rocks from Ascension Island, South Atlantic Ocean. *Journal of Petrology* **39**(5), 1009–1024.
- King, P. L., Hervig, R. L., Holloway, J. R., Vennemann, T. W. & Richter, K. (1999). Oxy-substitution and dehydrogenation in mantle-derived amphibole megacrysts. *Geochimica et Cosmochimica Acta* **63**(21), 3635–3651.
- Lindsley, D. H. & Nekvasil, H. (1989). A ternary feldspar model for all reasons. *EOS Transactions, American Geophysical Union* **70**(15), 506.
- Longhi, J. & Bertka, C. M. (1996). Graphical analysis of pigeonite–augite liquidus equilibria. *American Mineralogist* **81**, 685–695.
- Macdonald, R. (1964). A contribution to the island of Tutuila, American Samoa. *Geologische Rundschau* **27**, 821–837.
- Macdonald, R. (1974). The role of fractional crystallization in the formation of alkaline rocks. In: Sorensen, H. (ed.) *The Alkaline Rocks*. New York: John Wiley, pp. 442–458.
- Macdonald, R. (1987). Quaternary peralkaline silicic rocks and caldera volcanoes of Kenya. In: Fitton, J. G. & Upton, B. G. J. (eds) *Alkaline Igneous Rocks*. Boston, MA: Blackwell Scientific, pp. 313–333.
- Macdonald, R., Bailey, D. K. & Sutherland, D. S. (1970). Over-saturated peralkaline glassy trachytes from Kenya. *Journal of Petrology* **11**, 507–517.
- Mandeville, C. W., Webster, J. D., Rutherford, M. J., Taylor, B. E., Timbal, A. & Faure, K. (2002). Determination of molar absorptivities for infrared absorption bands of H₂O in andesitic glass. *American Mineralogist* **87**, 813–821.
- Mungall, J. E. & Martin, R. E. (1995). Petrogenesis of basalt–comendite and basalt–pantellerite suites, Terceira, Azores, and some implications for the origin of ocean island rhyolites. *Contributions to Mineralogy and Petrology* **119**, 43–55.
- Nekvasil, H. & Burnham, C. W. (1983). Thermodynamic modeling of crystallization paths of felsic silicate melts. *Geological Society of America, Abstracts with Programs* **15**(6), 651.
- Nekvasil, H. & Burnham, C. W. (1984). Thermodynamic modeling of crystallization paths in felsic melts; the haplogranite and haplogranodiorite systems. *Geological Society of America, Abstracts with Programs* **16**(6), 609.
- Nekvasil, H. & Burnham, C. W. (1987). The calculated individual effects of pressure and water content on phase equilibria in the granite system. In: Mysen, B. O. (ed.) *Magmatic Processes: Physicochemical Principles*. Geochemical Society, Special Publication **1**, 433–445.
- Nekvasil, H., Simon, A. & Lindsley, D. H. (2000). Crystal fractionation and the evolution of intra-plate *hy*-normative igneous suites: insights from their feldspars. *Journal of Petrology* **41**(12), 1743–1757.
- Newton, R. C., Charlu, T. V. & Kleppa, O. J. (1974). Calorimetric investigation of stability of anhydrous magnesium cordierite with

- application to granulite facies metamorphism. *Contributions to Mineralogy and Petrology* **44**(4), 295–311.
- Reiners, P. W., Nelson, B. K. & Ghiorso, M. S. (1995) Assimilation of felsic crust by basaltic magma: thermal limits and extents of crustal contamination of mantle-derived magmas. *Geology* **23**, 563–566.
- Schmincke, H. U. (1973). Magmatic evolution and tectonic regime in the Canary, Madeira, and Azores Island Groups. *Geological Society of America Bulletin* **84**, 633–648.
- Self, S. & Gunn, B. M. (1976). Petrology, volume and age relations of alkaline and saturated peralkaline volcanics from Terceira, Azores. *Contributions to Mineralogy and Petrology* **54**, 293–313.
- Stipp, J. J. & McDougall, I. (1968). Potassium–argon ages from the Nandewar volcano, near Narrabri, New South Wales. *Australian Journal of Science* **31**(2), 84–85.
- Stolz, A. J. (1985). The role of fractional crystallization in the evolution of the Nandewar volcano, North-eastern New South Wales, Australia. *Journal of Petrology* **26**, 1002–1026.
- Stolz, A. J. (1986). Mineralogy of the Nandewar volcano, Northeastern New South Wales, Australia. *Mineralogical Magazine* **50**, 241–255.
- Stout, M. Z., Nicholls, J. & Kuntz, M. A. (1994). Petrological and mineralogical variations in 2500–2000 yr BP lava flows, Craters of Moon lava field, Idaho. *Journal of Petrology* **35**, 1682–1715.
- Thompson, R. N. (1974). Some high-pressure pyroxenes. *Mineralogical Magazine* **39**, 768–787.
- Upton, B. G. J. & Emeleus, C. H. (1987). Mid-Proterozoic alkaline magmatism in southern Greenland: the Gardar Province. In: Fitton, J. G. & Upton, B. G. J. (eds) *Alkaline Igneous Rocks*. Boston, MA: Blackwell Scientific, pp. 449–471.
- Villari, L. (1975). The caldera of Pantelleria. *Bulletin Volcanologique* **34**, 658–766.
- Webster, J. D. (1997). Exsolution of Cl-bearing fluids from chlorine-enriched mineralizing granitic magmas and implications for ore metal transport. *Geochimica et Cosmochimica Acta* **61**, 1017–1030.
- Wellman, P. & McDougall, I. (1974). Potassium–argon ages on the Cenozoic volcanic rocks of New South Wales. *Journal of the Geological Society of Australia* **21**(Part 3), 242–247.
- Wellman, P., McElhinny, M. W. & McDougall, I. (1969). On the polar-wander path for Australia during the Cenozoic. *Geophysical Journal of the Royal Astronomical Society* **18**(4), 371–395.
- Wen, S. & Nekvasil, H. (1994). SOLVCALC; an interactive graphics program package for calculating the ternary feldspar solvus and for two-feldspar geothermometry. *Computers and Geosciences* **20**(6), 1025–1040.
- White, W. M., Tapia, M. D. M. & Schilling, J. G. (1979). The petrology and geochemistry of the Azores Islands. *Contributions to Mineralogy and Petrology* **69**, 201–213.
- Wright, J. B. (1969). Re-interpretation of a mixed petrographic province; the Sintra intrusive complex (Portugal) and related rocks. *Geologische Rundschau* **58**(2), 538–564.
- Zhou, F. (1994) Ti–Mg–Fe biotites: formation, substitution and thermodynamic properties at 650°C to 900°C and 1.1 kbar with fO₂ defined by the CH₄–C buffer. Ph.D. dissertation, State University of New York, Stony Brook.